# AB INITIO STUDY ON ELECTRONIC AND MAGNETIC PROPERTIES OF NANORIBBONS

by

Aseel AL MARMORI

A thesis submitted to

the Graduate School of Sciences and Engineering

of

Fatih University

in partial fulfillment of the requirements for the degree of

Master of Science

in

Physics

May 2014
Istanbul, Turkey

# APPROVAL PAGE

This is to certify that I have read this thesis written by Aseel AL MARMORI and that in my opinion it is fully adequate, in scope and quality, as a thesis for the degree of Master of Science in Physics.

_____
Assoc. Prof. Dr. Serkan ÇALIŞKAN
Thesis Supervisor

I certify that this thesis satisfies all the requirements as a thesis for the degree of Master of Science in Physics.

_____
Prof. Dr. Mustafa KUMRU
Head of Department

Examining Committee Members

Assoc. Prof. Dr. Serkan ÇALIŞKAN _____

Assoc. Prof. Dr. Ahmet ALTUN _____

Assist. Prof. Dr. Ali ŞAHİN _____

It is approved that this thesis has been written in compliance with the formatting rules laid down by the Graduate School of Sciences and Engineering.

_____
(Title and Name)
Director

May 2014

# AB INITIO STUDY ON ELECTRONIC AND MAGNETIC PROPERTIES OF NANORIBBONS

Aseel AL MARMORI

M.S. Thesis – Physics
May 2014

Thesis Supervisor: Assoc. Prof. Dr. Serkan ÇALIŞKAN

## ABSTRACT

The aim of this study is to understand the spin dependent properties of periodic and device nanoribbons. In particular, we concentrate on ZnO armchair and zigzag nanoribbons and compare them with C nanoribbons. The main purpose is to investigate the electronic and magnetic properties of these nanoribbons with different widths, through the spin polarized electrons. Using the ferromagnetic electrodes, spin dependent transport properties is also examined. The induced spin polarization is emerged either due to transition metal dopants or geometry of the nanoribbons. Hence, spin dependent behavior is revealed in these nano structures in the absence of external magnetic field. Both the spin dependent electronic and magnetic properties of nanoribbons are analyzed, employing *first principles* calculations through Atomistix ToolKit software. It is based on Density Functional Theory (DFT) combined with "Non-Equilibrium Green's Function Formalism" (NEGF). We obtain the relevant properties using the spin dependent band structure, conductance, transmission, density of states and magnetic moment. These results can be utilized to describe the nanoscale structures and stimulate the experimental works.

**Keywords**: Spintronics, Spin Polarized Transport, Density Functional Theory, ZnO Nanoribbons, C Nanoribbons, ZnO Device, C Device.

# NANOŞERİTLERİN ELEKTRONİK VE MANYETİK ÖZELLİKLERİ ÜZERİNE "AB INITIO" ÇALIŞMASI

Aseel AL MARMORI

Yüksek Lisans Tezi – Fizik
Mayıs 2014

Tez Danışmanı: Doç. Dr. Serkan ÇALIŞKAN

## ÖZ

Bu çalışmanın amacı periodik ve alet yapısındaki nanoşeritlerin spine bağlı özelliklerinin anlaşılmasıdır. Özellikle, "armchair" ve zigzag şeklindeki ZnO nanoşeritler üzerine konsentre olduk ve bunları C şeritlerle kıyasladık. Temel amaç, spin polarize elektronlarla, farklı genişliklerdeki bu şeritlerin elektronik ve manyetik özelliklerini araştırmaktır. Ferromanyetik elektrotlar kullanılarak, spine bağlı transport özellikleri de incelenmiştir. Meydana gelen spin polarizasyonu ya geçiş metali katkı atomlarından kaynaklanmakta ya da nanoşeritlerin geometrisinden kaynaklanmaktadır. Bunun sonucu olarak, dış manyetik alan yokluğunda, bu nano yapılarda spine bağlı davranış ortaya çıkmaktadır. "Atomistix ToolKit" paket programı vasıtasıyla *ilk ilkeler* hesaplamalarıyla nanoşeritlerin hem spine bağlı elektronik özellikleri hem de manyetik özellikleri analiz edilmiştir. Bu program Denge Dışındaki Green Fonksiyonu Formalizmi (NEGF) ile birleştirilmiş Yoğunluk Fonksiyonel Teorisi (DFT) tabanlıdır. We obtain the relevant properties using the spine bağlı bant yapısı, iletkenlik, transmisyon, durum yoğunluğu ve manyetik moment kullanılarak ilgili özellikler elde edilmiştir. Elde eldilen sonuçlar nano ölçekli yapıları tanımlamada ve deneysel çalışmaları teşvik etmede kullanılabilir.

**Anahtar Kelimeler:** Spintronik, Spin Polarize Transport, Yoğunluk Fonksiyonel Teorisi, ZnO Nanoşeritler, C Nanoşeritler, ZnO Alet Yapısı, C Alet Yapısı.

To my Family

# ACKNOWLEDGEMENT

First of all, I would like to express my appreciation to Assoc. Prof. Dr. Serkan ÇALIŞKAN for his great help and insight throughout the research, beside his patient and encouraging the whole time, it was great to work with him.

I am also thankful to my family for their understanding, motivation and patience. And to all my colleagues for the motivating atmosphere.

# TABLE OF CONTENTS

# LIST OF FIGURES

**FIGURE**

# LIST OF SYMBOLS AND ABBREVIATIONS

**SYMBOL/ABBREVIATION**

| | |
|---|---|
| ATK | Atomistix ToolKit |
| DFT | Density Functional Theory |
| $E^{xc}(\rho)$ | Exchange correlation energy |
| $E^{H}(\rho)$ | Hartree energy |
| $E^{ext}(\rho)$ | External energy |
| $E_{ee}$ | Electron electron interaction |
| $\varepsilon_F$ | Fermi level |
| $\epsilon_{xc}$ | Exchange correlation energy density |
| $\varepsilon$ | Single energy level |
| $F_{HK}(\rho)$ | Energy functional |
| $f_L(E), f_R(E)$ | Fermi distribution functions for the left and right electrodes |
| GF | Green's Function |
| GMR | Giant Magneto Resistance |
| H-K | Hohenberg Kohn Theorem |
| $H_{eff}$ | Effective Hamiltonian |
| $H_S$ | Hamiltonian of the scattering region |
| LDA | Local Density Approximation |
| MTJ | Magnetic Tunnel Junction |
| NEGF | Non-Equilibrium Green's Function Formalism |
| $\mu$ | Chemical potential |
| $T(E)$ | Transmission coefficient |
| TMR | Tunneling Magnetoresistance |
| VNL | Virtual Nanolab |

| | |
|---|---|
| $V^{eff}$ | Effective potenial |
| $V^{H}(\rho)$ | Hartree potenial |
| $V^{xc}(\rho)$ | Exchange-Correlation potential |
| $V^{ext}(\rho)$ | Electrostatic interaction in the system |
| $\psi$ | Wave function |
| $\rho(\vec{r})$ | Ground state density |
| $\sigma$ | Conductance |
| $\Sigma_L, \Sigma_R$ | Self energies of the left and the right probes |

# CHAPTER 1

# INTRODUCTION

The efficiency of improving technologies is the concern of materials scientist; as the need of it appeared with the end of silicon road map. Electrical devices depend on the electrical property of electrons. When a current is applied, the electron charge transfers the information with the current. Scientist found that another property of the electron, which is spin, can transfer the information, for instance, via a magnetic field. The study of the spin role lead to a new generation of electronic devices based on the flow of spin in addition to the flow of charge. It gives rise to the field known as spintronics or magnetoelectronics.

Spin dependent property is that researchers started to search in replacing conventional silicon, for modeling circuits, by more effective materials. The elaboration of devices is by carrying out processing and data storage on the same chip. It was found that movement of spin through some materials is more efficient as it is easily influenced through the magnetic field and has a coherent property for a sufficiently long time, needed in developing spintronic devices. One can have smaller devices that consume less energy and powerful using this property. Experimentally or theoretically, we need to examine certain materials to benefit from the spin property of electrons.

In this thesis, we intended to investigate the nanoribbons, in particular zinc oxide (ZnO) nanoribbons, to be able to get the advantageous results in studying the spin dependent properties. We compared the electronic structure properties of ZnO nanoribbons with those of carbon (C) nanoribbons. Nanoribbons containing transition metals with different concentration are also considered, as the transition metals play an important role in spin polarization. In general, we consider the electronic structure properties together

with magnetic ones. Transport behavior is determined through placing the systems between spin polarized semi-infinite electrodes. We applied the Atomistix ToolKit (ATK) software package in determining the spin dependent transport properties of nanoribbons. In this software, ab initio calculations are implemented via DFT (Density Functional Theory) combined with Non-Equilibrium Green's Function Formalism (NEGF).

This thesis is divided into 5 Chapters: In Chapter 2, we give a brief introduction of the theory; Chapter 3 introduces the computational method employed in software package ATK; Chapters 4 presents Results and Discussions of the spin dependent properties of ZnO and C nanoribbons; and Conclusion is presented in Chapter 5.

# CHAPTER 2

# THEORETICAL BACKGROUND

## 2.1 DENSITY FUNCTIONAL THEORY

In the microscopic world, where the electrons apply the particle-wave duality, quantum mechanics provides a mathematical description for their behaviors. Density functional theory (DFT) is one of the theories that works in the quantum mechanical world computations [Parr,1983]. It provides necessary information for describing systems, such as atoms, molecules and solids. The wave functions $\psi$ in such systems carry the whole information about them. Moreover, for a single electron the wave function is easy to possess through Schrödinger equation. When it comes to the many body problems neither it is easy to accomplish, nor we can predict the properties of the system through it. DFT emerged for this reason, where it is trying to simplify the many body problems.

DFT is a tool which utilizes the charge density. The charge density is a basic variable and the total energy becomes a functional of the density. DFT presented many theorems used to solve the Schrödinger equation for many body problems. Each one introduces a way in predicting certain property of a system depending on the boundary conditions. Schrödinger equation for a single particle under an external potential $v_{ext}(r)$ is

$$\left[\frac{\hbar^2\nabla^2}{2m} + v_{ext}(r)\right]\psi = E\psi \tag{2.1}$$

where $E$ is the total energy and $m$ is the mass of an electron.

For more than one particle (many body problem), the equation above becomes

$$[\sum_i^N [\frac{\hbar^2\ \nabla^2}{2m} + v_{ext}(r)] + \frac{1}{2}\sum_{i\neq j}^N \frac{e^2}{|r_i - r_j|}]\Psi(r_1, r_2, \dots r_N) = E\ \Psi(r_1, r_2, \dots r_N) \tag{2.2}$$

where the first term is the kinetic energy of the nuclei, the second term is the Coulomb interaction between the nuclei and each electron, the third term is the interaction energy between different electrons, Ψ is the wave function and $E$ is the total energy.

The first DFT theorem introduced is Hohenberg-Kohn (H-K) theorem [Hohenberg,1964]. The electron density $\rho$ is the main property studied by the theorem, where it is considered as the basic variable instead of the wave function in maintaining the properties of the system. Furthermore, it helps in finding the probability of electrons in a volume of $d^3\vec{r}$ in the system, where total number of electrons ($N$) is given by

$$N = \int \rho(\vec{r})\, d^3\vec{r} \tag{2.3}$$

The electron density fixes the external potential energy and, hence, determines the whole properties of the system as a function of density. For instance, the total energy $E(\rho)$ can be written as

$$E(\rho) = T(\rho) + E^{xc}(\rho) + E^{H}(\rho) + E^{ext}(\rho) \tag{2.4}$$

where $T(\rho)$ is the kinetic energy of Kohn-Sham orbitals (non-interacting particles), $E^{xc}(\rho)$ is the exchange correlation energy, $E^{H}(\rho)$ is the Hartree energy and $E^{ext}(\rho)$ is the external energy. The exchange correlation energy can be achieved only by the local density approximation (LDA) [Jones,1989].

$$E_{xc}^{LDA} = \int d^3\vec{r}\, \rho(r)\epsilon_{xc}(\rho(r)) \tag{2.5}$$

where $\epsilon_{xc}$ is the exchange correlation energy density.

In other words, H-K theorem determines the ground state properties, such as the ground state energy, the electronic density and the atomic structure. However, this can only be achieved if we have the ground state density $\rho(\vec{r})$. This is called the variation principle. The theorem introduces an energy functional $F_{HK}(\rho)$ used to prove that it can be minimized by the ground state density under a fixed potential energy

$$F_{HK}(\rho) = T(\rho) + E_{ee} \tag{2.6}$$

where $E_{ee}$ is the electron electron interaction.

The second theorem of DFT is Kohn-Sham (K-S) theorem [Kohn,1965]. The charge density and total energy are calculated through mapping the exact functional problem onto a pseudo single-particle Hamiltonian problem, known as the K-S Hamiltonian. It solves the many body problem by assuming non-interacting electrons under an effective potential

$$\hat{H}_{1el} = \frac{-\hbar}{2m}\nabla^2 + V^{eff}[\rho](r) \tag{2.7}$$

where $V^{eff}$ is the effective potential defined as

$$V^{eff}[\rho] = V^{H}[\rho] + V^{xc}[\rho] + V^{ext}[\rho] \tag{2.8}$$

Here the first term is the Hartree potential due to mean field electrostatic interaction, the second term is the exchange-correlation potential due to quantum mechanical nature of electrons and the last term represents the other electrostatic interactions in the system.

## 2.2 NON-EQUILIBRIUM GREEN'S FUNCTION FORMALISM

The Green's function (GF) theory is in help for understanding the quantum mechanical world beside the DFT. Its main function is to solve the Schrödinger equation for the transport through the systems, such as ballistic transport, where it takes into consideration the probability of electron transport between two probes (electrodes) to study the resulting scattering potential. This theory can only work for stationary states (*zero bias*), since no strong external field is applied. The information about the electronic structure and the scattering potential of the scattering region is not the main object of this theory. In the case of *finite bias*, the necessity of NEGF appears [Lake,1997]. NEGF has important applications within solid state, nuclear and plasma physics. Moreover, this function can provide time-dependent expectation values such as densities and current.

NEGF is based on calculation of the current between two probes while the information of the electronic structure and the scattering potential are preserved. For a simple model of two probes with different chemical potentials $\mu_1$ and $\mu_2$ attached to an atom (single energy level $\epsilon$), the resultant current is given by

$$I = \frac{e}{h}\int_{-\infty}^{\infty}[dE\ G(E)\gamma_1(E)G^*(E)\gamma_2(E)[f_1(E) - f_2(E)] \tag{2.9}$$

where $\gamma$ is the transmission rate, $G$ is the GF and $f$ is the Fermi function. In equilibrium where the energy level $E$ is equal to the single energy level $\epsilon$, the Fermi function for the first contact between the probe and the system is given by

$$f_1(\epsilon) = \frac{1}{1+e^{\frac{(\epsilon-\mu_1)}{\kappa_B T}}} \tag{2.10}$$

and we have the same expression for the second contact between the probe and the system. From the equation of current, we see that the current mainly depends on the GF. It is a powerful analytical tool and defined by the energy as

$$G(E) = \frac{1}{E-\epsilon+\frac{i\gamma}{2}} \tag{2.11}$$

NEGF generalizes the above simple model by including the effective Hamiltonian $H_{eff} = H_S + \Sigma_1 - \Sigma_2$ , where $\Sigma_1 - \Sigma_2$ are the self energies for the left and right probes and $H_S$ is the Hamiltonian of the scattering region. $H_{eff}$ carries the detailed information needed, as $\Sigma$ tells about the electronic structures of the probes and their relations with the scattering region where the system is located. So the generalized GF becomes

$$G(E) = \lim_{\eta\to 0}[((E + i\eta) - H_S - \Sigma_1 - \Sigma_2)^{-1}] \tag{2.12}$$

where, $\eta$ is a causality factor.

## 2.3 SPINTRONICS

Devices have been improved over the time to accept data as input, process it and serve results as output.

One of the main integrated devices for this reason in the past was transistors, which have been developed to microprocessors over the years. Information can be transported through it by the electric charge as it is expressed in binary digit, where (0, 1) represents the absence or existence of the electric charge.

Efforts have been applied to increase the capability of integrated factors by the applicable materials, like semiconductors or metals. Such increase was due to applying Moor's law [Moore,1998]. This law states that microprocessors will double in power every 18 months as electronic devices shrink, where more logic is packed into every chip. Silicon (Si) has been the most widely used to construct microelectronics circuits as it is dependable and cost-efficient, even though it no longer applies the Moors law. The size of the individual bits approaches the dimension of atoms; indicating the minimum possible size of the chips. Therefore the necessity of enhancing the functionality of devices in other ways appeared. This can be exploited by another property of the electron: *spin* [Chambers,2002].

It was found that the transportation of information through the movement of spin in circuits is more efficient, as it can be manipulated through the magnetic field and has a coherent property which lasts for a long time. Introducing the spin can result in smaller devices, consuming less electricity and powerful for certain types of computation. Spin relaxation (how a spin produces and disappears) and spin transport (how a spin moves in metals and semiconductors) are the main two things that need to be taken into account as they play important role in electronic technology.

The devices based on spin transportation are called spintronic devices. The first spintronic device was the one which exposed Giant Magneto Resistance (GMR) [Baibich,1988]. It consists of ferromagnetic and non-magnetic layers. Depending on the relative magnetization in the magnetic layers, the electrical resistivity of the device changes from small values (*parallel magnetization*) to large values (*anti-parallel magnetization*). This device is currently used in a computer hard-disk platter, where its prosperity has been proved in storing data.

Researchers are now working on two main points; the first is to advance the exciting GMR, while the second is to find new ways both to generate and employ the spin-polarized currents.

Spintronic devices made of semiconductors are more efficient as they are flexible, the band gap can be controlled and existing potential barrier works as a switch. In addition it provides amplification and serves as multi-functional devices. Perhaps even more importantly, semiconductor-based devices could much more easily be integrated with traditional semiconductor technology. The problem in metal based devices is that they do not amplify signals and have a potential barrier.

Metal-oxide-semiconductor technology was the first scheme for spintronic devices. In a conventional field effect transistor, electric charge is introduced via a source electrode and collected at a drain electrode. A third electrode, the gate, generates an electric field that changes the size of the channel through which the source-drain current can flow. Datta-Das transistor [Datta,1990] is a spin field effect transistor, where, for instance, indium-aluminum-arsenide and indium-gallium-arsenide provides a channel for two-dimensional electron transport between two ferromagnetic electrodes. One electrode acts as an emitter and the other as a collector. Basically, the realization of such a device requires achieving both efficient spin-injection from a ferromagnetic electrode into a semiconductor and spin-detection of a polarized current passing from the semiconductor into other ferromagnetic electrode. When the system used between the ferromagnetic electrodes is metal, the device then becomes metal spin transistor and works in the same principle of GMR.

Tunnel Magnetoresistence (TMR) [Yuasa,2007] is another spintronic device where an insulator is sandwiched between the two ferromagnetic electrodes. When the insulator is thin enough the electrons can transport easily from source electrode to the other one. Magnetic Tunnel Junction (MTJ) [Meng,2005] is a device which has at least two magnetic layers separated by an insulating tunnel barrier.

## 2.4 QUANTUM TRANSPORT

The transportation of electrons through a microscopic system in a device should be studied quantum mechanically, as the size of the device becomes comparable to the Fermi wave length. Therefore, some properties such as the *spin polarization* cannot be neglected. When the net spin of the electrodes is not zero, we have non-equilibrium

spin, as a result when a voltage is applied to the ferromagnetic electrods spin current engenders. The transport of non-equilibrium spin across the interface (between an electrode and the system) is called spin injection. The electrons may encounter potential barrier across the interface, in this case *diffusive transport* happens. Barriers exist in semiconductors as a result of impurities and strongly depend on bias between the electrodes and doping. Electron tunneling cause loss in energy and information as a result of spin-orbit coupling [Jaroslav,2009]. On the other hand *ballistic transport* happens when there are no potential barriers. Hot electrons (higher energy level than the potential barrier) can overcome the potential barrier of the interface.

The spin transport can be studied at the atomic scale through introducing the point contact model, where the non magnetic systems such as atoms, molecules or polymers are sandwitched between two ferromagnetic electrodes. The spin relaxation can be sufficiently long in this model if the electrons encounter the same spin orienation for a long time.

The degree of spin injection in the non magnetic region depends on the conductivities of the ferromagnetic electrodes (F) and the non magnetic one (N). When the conductivity of F region is less than N region, the effeciency of the spin injection is higher, the opposite is also true. The conductance ($\sigma$) depends on the transport properties of the system. It is given by the sum of all the transmission probabilities ($T$) through the whole quantum channels of the system (scattering region) that connects the electrodes, the relation between the conductance and the transmission probability is given by

$$\sigma = \frac{e^2}{h} \sum T \tag{2.13}$$

The injection of non-equilibrium spin either induces voltage or changes resistance depending on the build-up of the non-equilibrium spin. Moreover, the spin diffusion length depends on two factors; the thickness of the system and the spin life time (the time it keeps its spin orientation). In our thesis, we assume perfect injection without potential barrier between the electrodes and the system.

## 2.5 NANORIBBONS and ZnO NANORIBBONS

The study of the materials while changing their dimension took the attention of the materials scientists, as they noticed the changes in electronic and magnetic properties along with it. The structures of the materials can be of 0D (Quantum Dot), 1D (wire), 2D (sheet) or 3D (bulk). Each of these structures shows different properties. In addition, the performance of any constructed device can be affected by some factors such as intelligent surface, amplification, synthesis methods and the shape [Tiwan.et.al, 2012].

Graphene is a 2D crystalline allotrope of carbon, where atoms are densely packed in hexagonal pattern [Meyer,2007]. C materials as nanostructures manifest prodigious properties depending on their geometry. Moreover, from graphene sheets *C nanoribbons* can be made. C nanoribbons are quasi 1D nanometer-sized stripes of less than 50 nm. In the present thesis nanoribbons structures are considered. In particular, we have focused on ZnO nanoribbons. It has a graphitic like structure, meaning it is hexagonally crystallized, also called as honey comb cell structure. The edge of this structure can be one of two shapes: *armchair* or *zigzag* (see Figure 2.1).

The geometry of a ZnO nanoribbon plays significant role in the properties of a relevant system, where some studies, both computationally and experimentally, have already been investigated on its stability [Topsakal,2009]. Regarding the geometry, two kinds of edges, armchair and zigzag, have been taken into consideration. These two different edges control some properties of the system. For instance, single layer of zigzag ZnO nanoribbon shows metallic behavior while armchair ZnO nanoribbon exhibits semiconductor property [Botello-Mendez,2007]. In addition, the width and the thickness of the system are crucial in controlling the electronic properties of the system. Increasing the width of the system, for instance, raises the electron scattering during the electron motion [Lamba,2012]. Figure 2.2 shows the two types of a ZnO nanoribbon, constructed using the Virtual NanoLab (VNL) in Atomistix ToolKit (ATK) software [Atomistix ToolKit, version 2011].

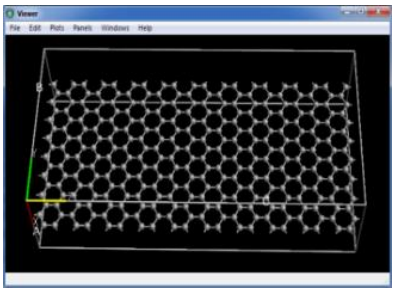

(a)

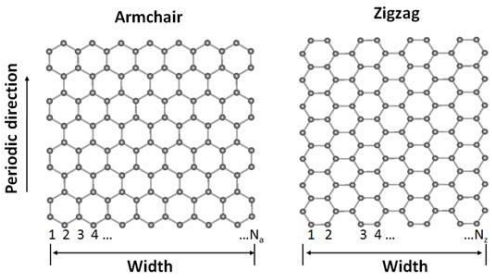


(b)

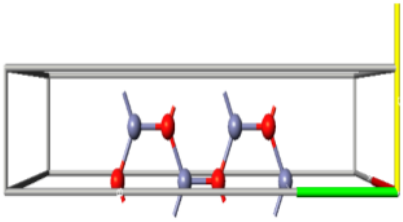

(c)

Figure 2.1 Nanostructuers are shown in different geometries. (a) 2D graphene sheet, (b) C nanoribbons, which are constructed from the graphene sheet where the two kinds of edges are shown, (c) ZnO nanoribbon unit cell where the blue atom represents the zinc and the red one stands for the oxygen atom.

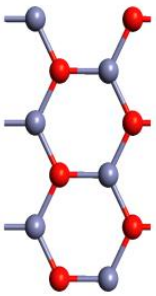

(a)

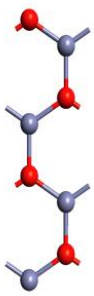

(b)

Figure 2.2 Quasi one dimensional nanoribbons of a ZnO based system with two kinds of edges. (a) Armchair ZnO nanoribbon and (b) Zigzag ZnO nanoribbon.

# CHAPTER 3

# SOFTWARE PACKAGE

## 3.1 ATOMISTIX TOOLKIT

Atomistix ToolKit (ATK) [Atomistix ToolKit, version 2011] is a tool that expounds the basic principles of atomic scale modeling in general, quantum transport calculations in particular. It is vastly employed in industrial and academic areas because of its advantages in applications. It deals with several aspects of these areas ranging from the basic properties to constructed devices applications such as spintronics. Generally, common procedures are applied for the required results, starting from setting geometry for the model in hand. This can be realized by what so called Virtual NanoLab (VNL). It is a graphical user interface in ATK that is very useful in constructing the structures and extracting the data from the calculations. These calculations can be carried out upon applying numerical model with certain parameters to the constructed geometry. The procedures are related to the atomic scale modeling, while for the quantum transport a connection between two surfaces is needed. In addition, one can introduce defects and study the current-voltage characteristic of an atomic structure between the electrodes.

ATK employs the *python* as its programming language, which is a well-known language in the scientific field. Through the python, in ATK one is able to develop more advanced geometry setups, analysis functions and to play with the built in parameters. In other words, ATK provides techniques for simulating nanostructures on atomic scales. Moreover, it is capable of applying theories such as DFT, tight binding model and NEGF on any structure, in order to demonstrate basic properties or manipulate specific device applications.

Nevertheless, through having an ideal system one can accomplish the basic principles of both electronic structure and quantum transport.

### 3.1.1 Device Configuration

Device configuration is a two probe system formed by two electrodes and a system between them. Using the VNL, as mentioned above, the system to be considered is connected between two surfaces to extract and manipulate the transport properties. The system or sample can be of many forms depending on its shape or dimension. For instance, C nanotube as 1D, infinite graphene sheet as 2D, graphene and ZnO nanoribbons as stripes. The two surfaces located on the left and right are the parts of bulk configuration of two electrodes, a sandwich or two probe model. Figure 3.1 shows this model for a graphene nanoribbon between the two electrodes, forming an electronic device. The configuration in this figure manifests the parts of such a sandwiched geometry; the electrodes extensions and the *scattering region* where the geometry is not bulk-like. The electrode extensions and scattering region form the interaction region, through which one can apply a bias between the left and right electrodes.

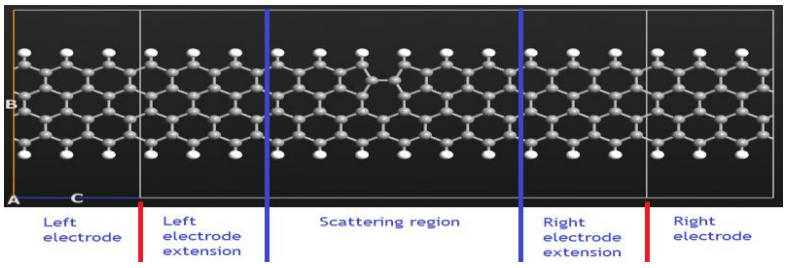


Figure 3.1 A graphene nanoribbon device constructed in VNL. It consists of left and right electrodes and interaction region in between. The interaction region contains the electrode extensions and scattering region.

In ATK the techniques, theories and the simulations are usually applied on the scattering region, in order to have clear vision about the need to know properties, such

as electronic structure and the quantum transport. The extensions of the electrodes work as leads, consisting of transport channels, which are responsible of the conductance and the transmission. The scattering region is the key for composing device characteristics. For instance, forming diodes by adding dopants or introducing defects to the scattering region would lead to the in-demand electronic properties.

The device constructed in VNL must contain the electrodes in addition to the interaction region mentioned above. A device has its own characteristics depending on the structures of the contained parts. For instance, the left and right electrodes (known as source and drain) can be metal surfaces such as nickel or gold. A graphene sandwiched between, them introduces a Magnetic Tunnel Junction (MTJ). Mainly, the functionalization of the device can be controlled through a modification in the electronic properties of the scattering region. This can be done via introducing dopants, defects or even bonds of the contained system.

## 3.2 THE PROPERTIES OF ATK

ATK offers many features required to test the functionality of certain models in industrial and research areas. The main concerned properties are the electronic, magnetic, optical, thermal and the transport properties. The electronic properties are of interest in how the electronic structure affects the device behavior, for instance, metallic or semiconductor property. The band structure and the density of states are the common electronic properties studied by ATK, as they provide sufficient required information.

*The band structure* is a schematic that tells about the range of energies the electron may or may not have. It is divided into three parts, the valence band, band gap and the conduction band. The valence band and the conduction band represent the range of energies the electron can occupy, while the band gap is the range of energies the electron cannot occupy. The main information read from the band structure is the electronic behavior of a material. For instance, an overlap between the conduction band and the valence band with zero band gap yields the metallic behavior, on the other hand one obtains an insulator when a large separation appears between the two bands.

Figure 3.2 shows the band structure of graphene. In the present thesis, Fermi level $\varepsilon_F$ is set to zero. From the figure shown we observe a metallic behavior due to the overlap between the valence and the conduction bands. Γ and Z points in the diagram represent the symmetry points of the wave vector $k$ along the first *Brillion zone* from the periodic structure.

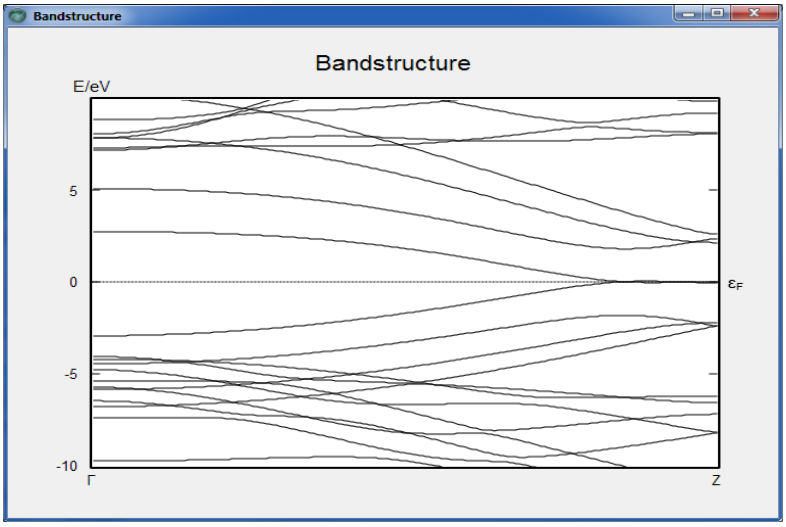


Figure 3.2 The band structure of graphene. An overlap observed at the Fermi level close to the Z point means that graphene exhibits metallic behavior.

Another important property for the materials under investigation is the transport property, where the *I-V characteristics* and the *transmission spectrum* are of concern. *I-V* curve describes the relation between the current and the corresponding applied bias voltage between the electrodes. The current can be found from the transmission spectrum, through Landauer's formula [Landaueri,1957]

$$I = \frac{2e^2}{h} \int \mathrm{T}(E, V_\mathrm{b})[f_\mathrm{L}(E) - f_\mathrm{R}(E)]\mathrm{d}E \tag{3.1}$$

where, e is the electron charge, $f_\mathrm{L}(E), f_\mathrm{R}(E)$ are the Fermi distribution functions for the left and right electrodes, respectively and $\mathrm{T}(E, V_\mathrm{b})$ is the transmission coefficient. A perfect transmission spectrum can be obtained when no defects are introduced to the system. A perfect transmission spectrum for the graphene nanoribbon is shown in Figure 3.3, where we see a pronounced peak at the Fermi energy.

The density of states (DOS) is defined as the number of the available states for an electron to occupy at certain energy. Figure 3.4, shows the DOS of a bulk Si calculated through ATK. The zero DOS around the Fermi level $\varepsilon_F$ implies the semiconducting behavior.

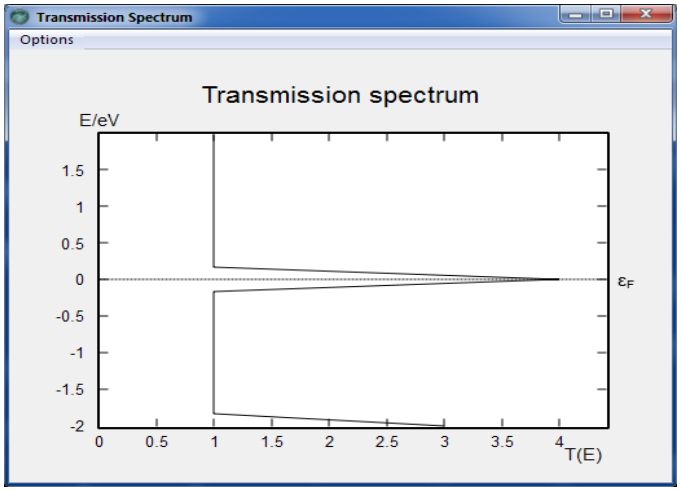


Figure 3.3 The transmission spectrum of a graphene nanoribbon containing no defect.

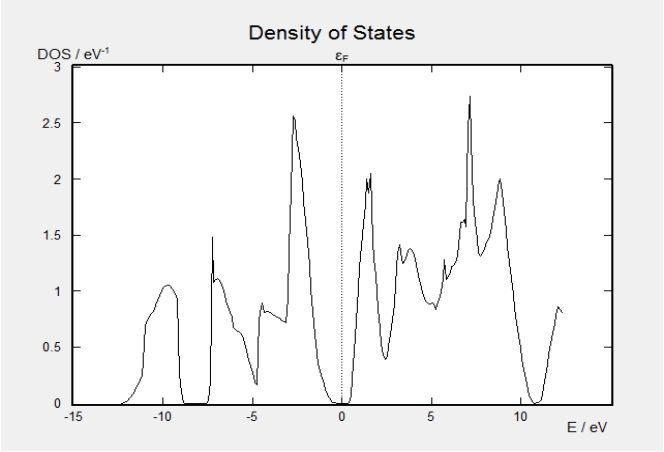


Figure 3.4 The density of states of a bulk Si obtained by ATK.

One of the interesting properties that make the ATK a distinctive software is the ability to investigate the spin dependent properties of novel materials using *first-principles* methods. It enables us to calculate, for instance, spin dependent *I-V* characteristics, conductance, spin polarization, voltage drop, TMR etc.

# CHAPTER 4

# RESULTS AND DISCUSSIONS

## 4.1 ELECTRONIC and MAGNETIC PROPERTIES OF NANORIBBONS

The main goal in our thesis is to maintain the electronic properties for the nanoribbons with respect to some factors, such as molecular structure, spin, width, doping and distortion. Two kinds of nanoribbons have been choosen for the study: ZnO nanoribbons and C nanoribbons. The calculations have been performed on these two systems by ATK, and in the following we will present some results.

First, the geometry of each system was constructed using the Builder in ATK. For both the armchair and the zigzag nanoribbons, the corresponding electronic structure properties were revealed in the presence and the absence of spin. Then, the effect of width was considered comparing two nanoribbons with different widths. Moreover, the influence of *k points* was also analyzed for a particular system.

Employing the ZnO nanoribbons, device configuration (two probe system) was constructed, for both the armchair and the zigzag types. Then the relevant quantities (transmission spectrum, density of states, conductance etc.) were obtained for different widths. Especially, the effect of ferromagnetic electrodes was studied by using Ni for the armchair nanoribbon.

As for the C nanoribbons, both armchair and the zigzag C nanoribbons were investigated. Then, in a similar manner, the electronic structure calculations were carried out both in the presence and the absence of spin. Effect of width was also considered for the armchair C nanoribbons. In addition, we compared the results for device configurations with and without distortion.

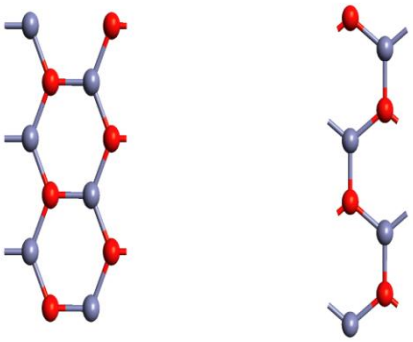

(a) (b)

Figure 4.1 Two different structures of a ZnO nanoribbon. (a) Armchair nanoribbon, where Zn (blue) and O (red) atoms are located on the inner and outer edge, respectively, and they are alternating along one direction; (b) Zigzag nanoribbon, where a pair of Zn and O atoms are located, in turn, on the right and left side.

## 4.2 SPIN DEPENDENT ELECTRONIC and MAGNETIC PROPERTIES OF ZnO NANORIBBONS

ZnO nanoribbons with two different geometries, which are the armchair and the zigzag type, are illustrated in Figure 4.1. Figure 4.1 indicates the unit cell of these structures, where the arrangenment of Zn and O atoms controls the geometry or shape of the ZnO nanoribbons. In an armchair nanoribbon, Zn and O atoms are located on the inner and outer edge, respectively, and they are alternating along one direction (see Figure 4.1a). As for the zigzag nanoribbon, a pair of Zn and O atoms are placed, in turn, on the right and left side of the structure (see Figure 4.1b). We performed the calculations for these geometries, both in the absence and the presence of spin. The spin dependent electronic structure properties of the systems exhibit themselves through the asymmetric variations of the spin states in the obtained spectra.

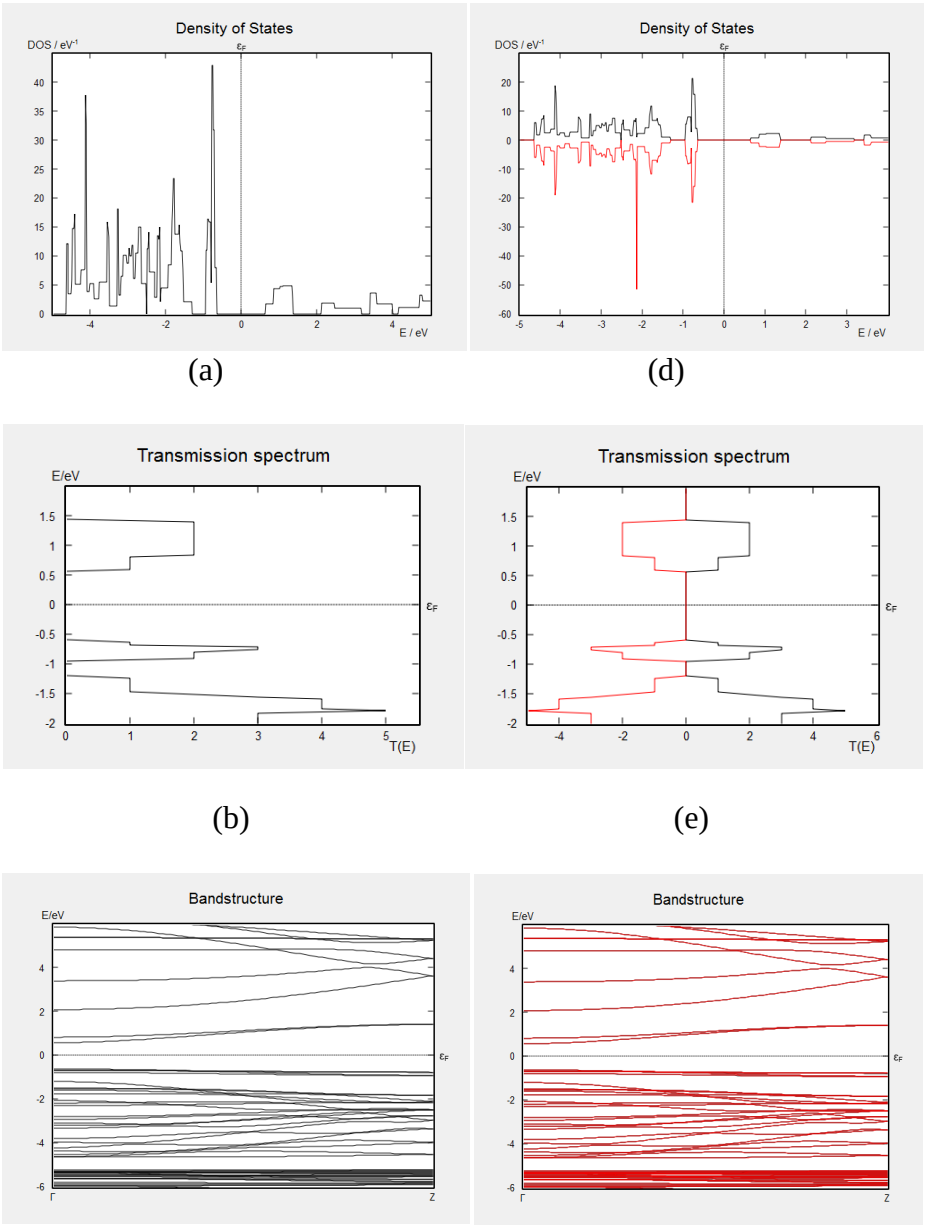


Figure 4.2 The results for an armchair ZnO nanoribbon in the absence and presence of spin. (a), (b) and (c) are the density of states, transmission spectrum and the band structure in the absence of spin, respectively; (d), (e) and (f) density of states, transmission spectrum and the band structure in the presence of spin, respectively.

Figure 4.2 shows a comparison of the armchair ZnO nanoribbons both in the absence and presence of spin. Spin independent results are shown in Figure 4.2a, b and c. Spin dependent results are illustrated in Figure 4.2d, e and f, where spin up (majority) states are denoted by black (positive values) and spin down (minority) states are shown by red (negative) for the sake of clarity. The absence of density of states around the Fermi level (which is set to zero in all diagrams) for both spin directions indicates the semiconducting behavior as shown in Figure 4.2a and d. Nanoribbons are the examples for the quasi one dimensional systems. One of the properties of a one dimensional system is that the transmission spectrum exhibits step like variation. Therefore, this step like behavior in transmission spectrum was observed for both majority and minority spins in our results (see Figure 4.2 b and e).

The zero transmission at the Fermi level implies zero conductance in the absence of applied voltage (zero bias conductances). The majority and minority electronic band structures are shown in Figure 4.2c and f. From the band structure, it is seen that the armchair nanoribbons exhibit a semiconducting behavior. The direct band gap was found as 1.2 eV for both majority and minority spins. From the spectra in Figure 4.2, we observed that armchair ZnO nanoribbon has a direct band gap and reveals spin symmetry (majority and minority spin variations are identical). Thus, there is no spin polarization induced or spin dependent behavior for this structure.

The Hubbard correction (U) is a term added to the exchange-correlation energy in DFT calculations [Hubbard,1963]. This term works on minimizing the total energy of the system by taking into account the deficiencies of the local exchange-correlation functional. The most known deficiency of DFT is to underestimate the band gap, which may lead to incorrect electronic structure results. U term makes a crucial correction in some systems. In the present thesis, the impact of it was studied via comparing the armchair ZnO nanoribbon properties in absence and presence of this term. In the electronic band structures, a slight difference was observed in the band gap value upon taking into account U term (see Figures 4.2f and 4.3c). The direct band gap in the presence of U correction was found to be 1.29 eV with spin symmetry. Also, a semiconducting behavior was observed for this system, as a result of an absence in the spin density of states at the Fermi level, which was also evidenced by a zero

transmission coefficient in the transmission spectra at the Fermi level (see Figure 4.3a and b).

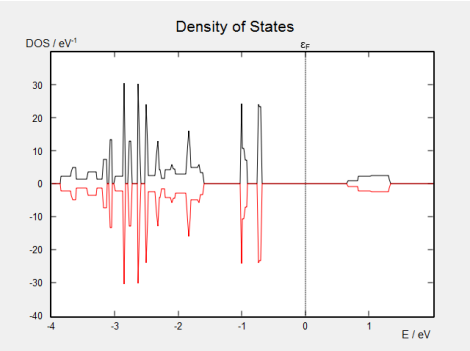


(a)

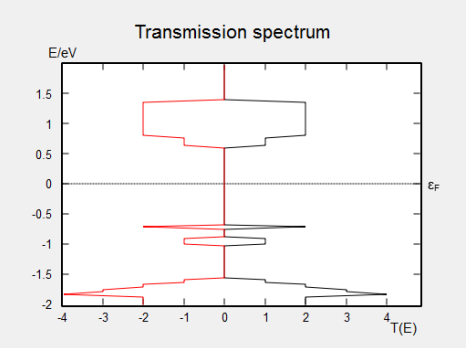


(b)

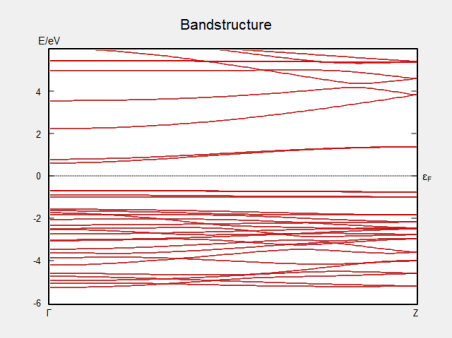


(c)

Figure 4.3 The results for an armchair ZnO nanoribbon in the presence of U correction.(a), (b), (c) the transmission spectrum, spin dependent density of states and the band structure, respectively.

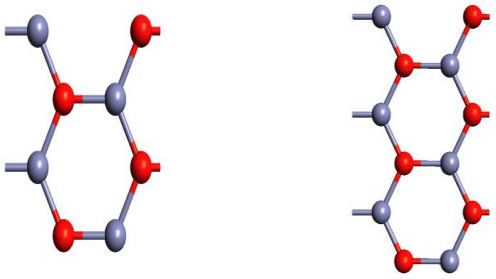

(a) (b)

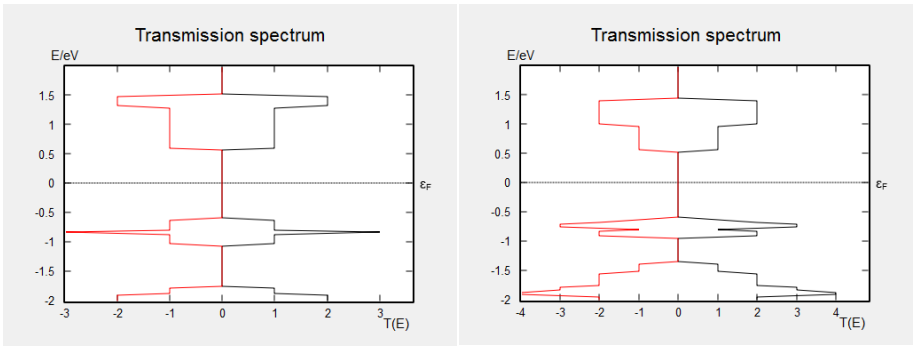


(c) (e)

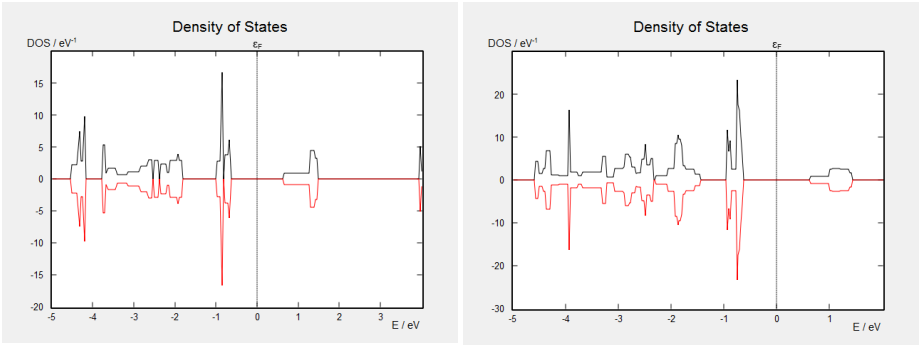


(d) (f)

Figure 4.4 The results for an armchair ZnO nanoribbon with the widths defined by $W_4$ and $W_6$ (see the text). (a) and (b) represent the geometries of $W_4$ and $W_6$, respectively; (c), (d) Transmission spectrum and density of states of $W_4$; (e), (f) Transmission spectrum and density of states of $W_6$.

After figuring out the electronic properties in the absence and the presence of spin for the afore mentioned structure, the effect of width was also examined. In Figure 4.1a, the armchair ZnO nanoribbons had a width of 11.52 Å ($W_8$, which is the default structure consisting of 8 atoms along the width). In addition, the electronic properties of a ZnO nanoribbon with two different widths were also examined for the sake of comparison. The structures shown in Figure 4.4a and b have a width of 4.93 Å ($W_4$, a structure consisting of 4 atoms along the width) and 8.22 Å ($W_6$, a structure consisting of 6 atoms along the width), respectively. It is seen in Figure 4.4 that the electronic properties are close to each other around the Fermi energy even if there are some qualitative distinct variations for the whole energy interval. As in the case of $W_8$, the spectra are spin symmetric for $W_4$ and $W_6$. Thus spin symmetric variation is not destroyed through the width of nanoribbons. The absence of density of states around the Fermi level is seen in Figure 4.4d and f, indicating the semiconducting behavior. The direct band gap value wasn't modified as a function of system width and was found to be 1.2 eV.

The *k points* represent Brillouin zone sampling, related to reciprocal vector. For bulk systems and electrodes, the numbers represent the *k points* along each vector. ($(k_1, k_2, k_3)$ Are the set of points which inform how many points should be utilized along the three directions of a unit cell vector. These points can control the accuracy of the calculations, where increasing the numbers of *k points* raises the accuracy of the calculations. However, it also increases the calculation time. Thus one needs to pay attention to defining the *k points* before running the calculations. For a particular system, we compared the *k points* to see the effects of them on the results by comparing the electronic structure properties for both $k_9$, representing the (9,9,9), and $k_{12}$, representing the (12,12,12). A slight difference arises in the results after increasing the points. Figure 4.5 shows the electronic properties of armchair ZnO nanoribbon for the $k_9$ and $k_{12}$. For instance, the direct band gap for $k_9$ and $k_{12}$ were found to be 1.1 eV and 1.2 eV, respectively (Figure 4.5c and f). Moreover, there are some qualitative differences in the density of states due to $k_9$ and $k_{12}$. We observed changes in the height of peaks even if general behavior is the same in the vicinity of the Fermi level (Figure 4.4a and d). In the present thesis, for periodic and two probe systems the default

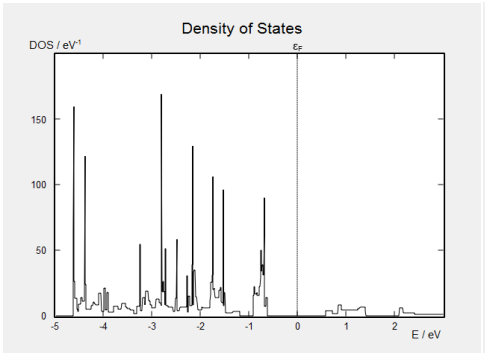


(a)

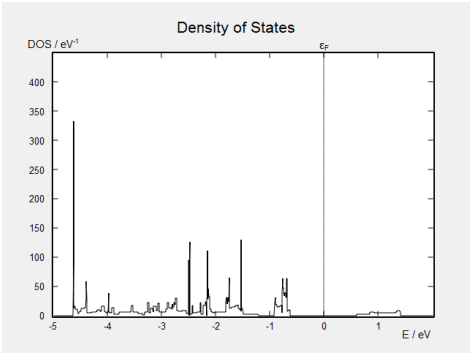


(d)

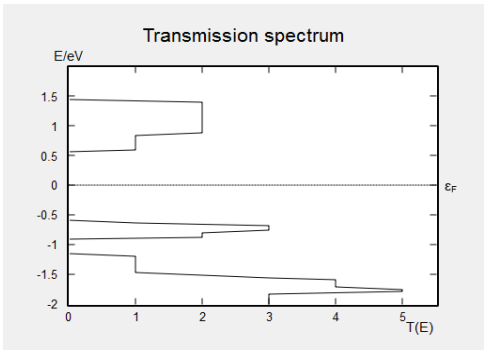


(b)

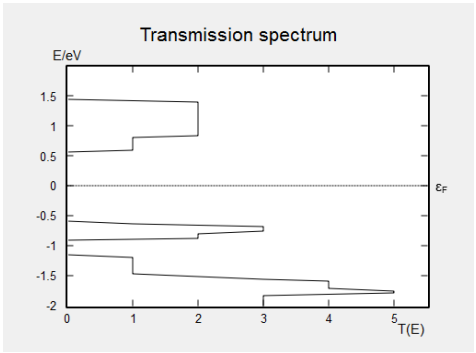


(e)

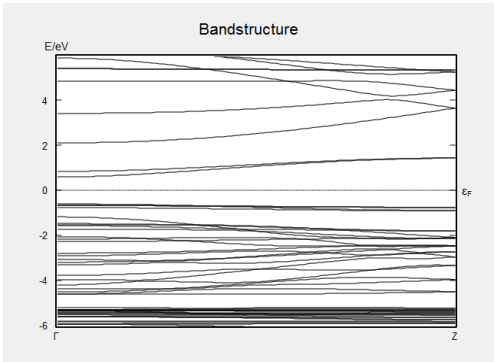


(c)

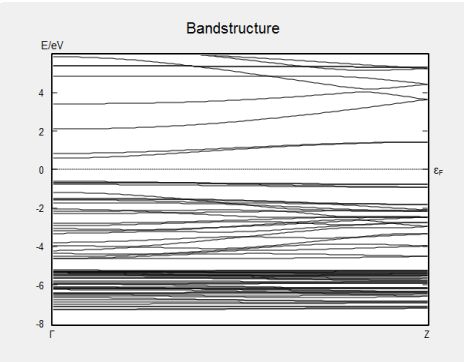


(f)

Figure 4.5 The results for an armchair ZnO nanoribbon for two different *k points*. The density of states, the transmission spectrum and the band structure results for $k_9$ in (a), (b) and (c) and for $k_{12}$ in (d), (e) and (f).

*k points* were taken as $k_6$ = (6,6,6) and (6,6,100). Since they give the sufficient accuracy, in order to get rid of time consuming, one doesn't need to take into account the higher *k points*.

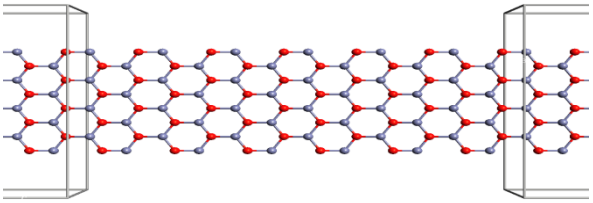

(a)

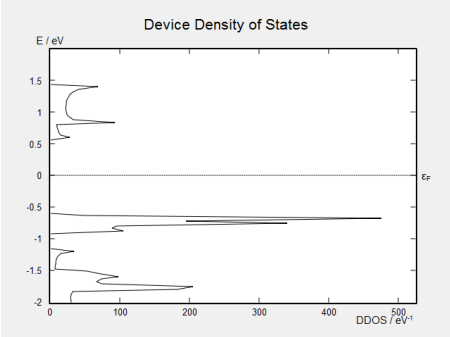


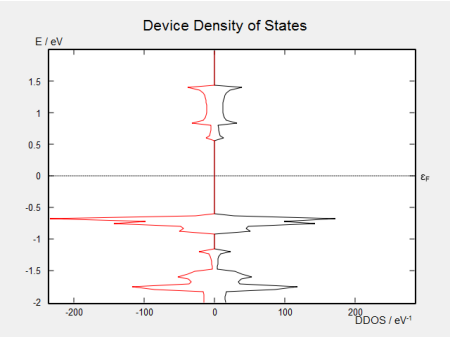


(b) (d)

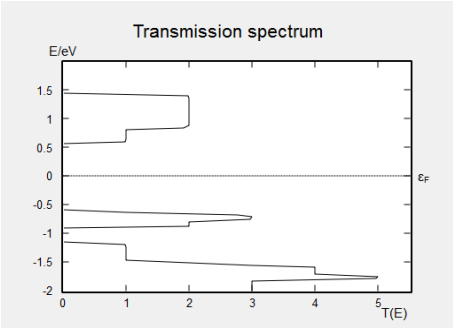


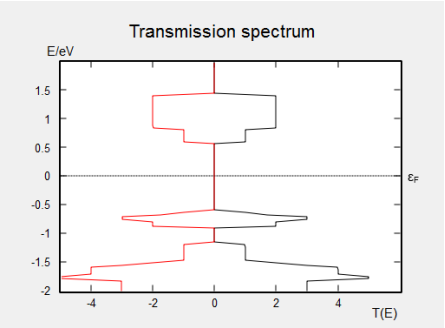


(c) (e)

Figure 4.6 The results for an armchair ZnO nanoribbon device. (a) The geometry of the device; the device density of states and the transmission spectrum in the absence of spin in (b), (c) and in the presence of spin in (d), (e).

For an armchair ZnO device structure (both the electrodes and the central region contain armchair ZnO nanoribbon), the main electronic structure properties were analyzed both in the absence and the presence of spin (see Figure 4.6). First, we observed a spin symmetric transport behavior through the pure prefect ZnO device. The semiconducting transport was obvious as illustrated in Figure 4.6b and d. The transmission spectra in Figure 4.6c and e imply that the conductance becomes zero at zero bias. The variation in the device density of states is consistent with that in transmission as seen in Figure 4.6b-e. The transmission is related to both the electrodes and electronic structure of the system in the central region; however density of states corresponds to the system attached to the electrodes. Thus, a finite density of states at certain energy doesn't always imply a finite transmission. The calculation on the average magnetic moment was also performed via Mulliken population (Mulliken, 1955). For the armchair ZnO device in Figure 4.6a, the average magnetic moment per central atom was obtained to be $1.70\text{x}10^{-8}\mu_B$ ($\mu_B$ is the Bohr magnetron) and the average magnetic moment per atom was $-2.71\text{x}10^{-7}\mu_B$. The positive value of the magnetic moment indicates that majority spin contribution is greater than minority one. We see that the magnetic moment is almost zero, which is a consequence of spin independent behavior of the structure.

Then, the presence of Hubbard correction U for the armchair ZnO device was examined as shown in Figure 4.7. It was found that the average magnetic moment per central atom and per atom becomes $3.58\text{x}10^{-8}\ \mu_B$ and $4.44\text{x}10^{-8}\ \mu_B$, respectively. Note the magnetic moment values without U for this device to see the obvious effect of U term. Even if the magnetic moment values with U become higher than those obtained in the absence of U, all of them are close to zero which implies nearly spin independent behavior for armchair ZnO nanoribbon devices.

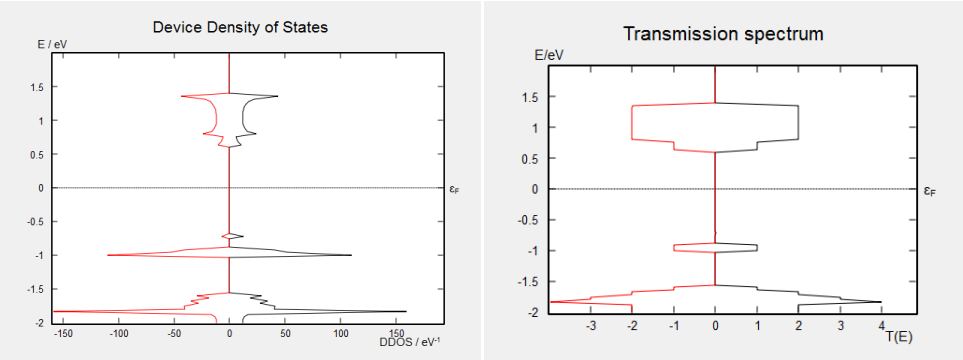


(a) (b)

Figure 4.7 The results for an armchair ZnO nanoribbon device in the presence of U correction. (a), (b) The device density of states and the transmission spectrum, respectively.

The effect of distortion on the spin dependent transport was investigated through removing a few atoms in the central region of armchair ZnO nanoribbon device (see Figure 4.8a). The semiconducting property is clear from the density of states spectra around the Fermi level as shown in Figure 4.8b. It was observed that the spin symmetric variation (For instance, see Figure 4.6e) modified to spin asymmetric behavior in the presence of distortion (see Figure 4.8c). It indicates the effect of geometry on the spin dependent behavior or spin polarization. The induced average magnetic moment values per central atom and per atom (including electrodes) were $1.37\text{x}10^{-3}\mu_B$ and $8.72\text{x}10^{-5}\mu_B$, respectively.

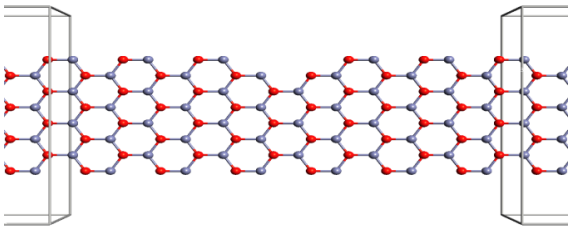

(a)

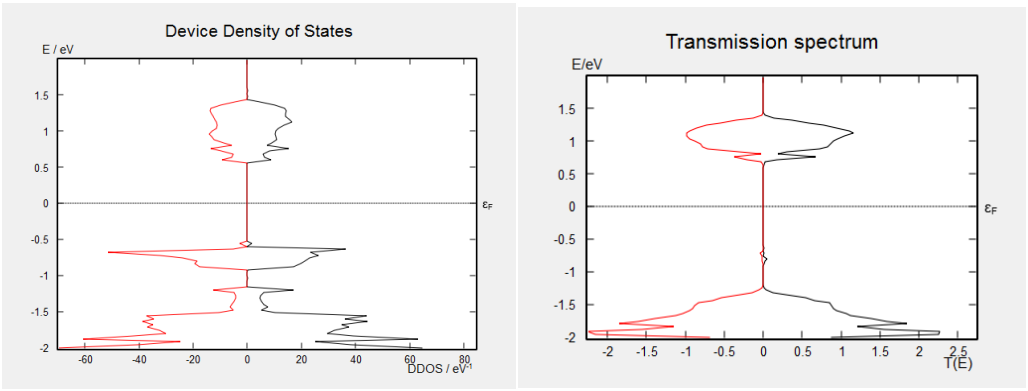


(b) (c)

Figure 4.8 The results for a distorted armchair ZnO device. (a) The geometry of a distorted armchair ZnO nanoribbon device; (c), (d) The density of states and the transmission spectrum of this device.

The effect of width of an armchair ZnO device on the spectra was also examined via $W_4$ and $W_6$ as shown in Figure 4.9a and b. The zero transmission in the vicinity of the Fermi level implies the semiconducting behavior in the absence of bias voltage. No crucial change was observed in the transport behavior as shown in Figure 4.9c and e.

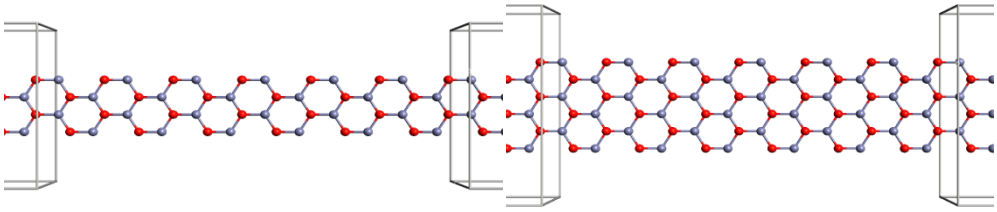

(a) (b)

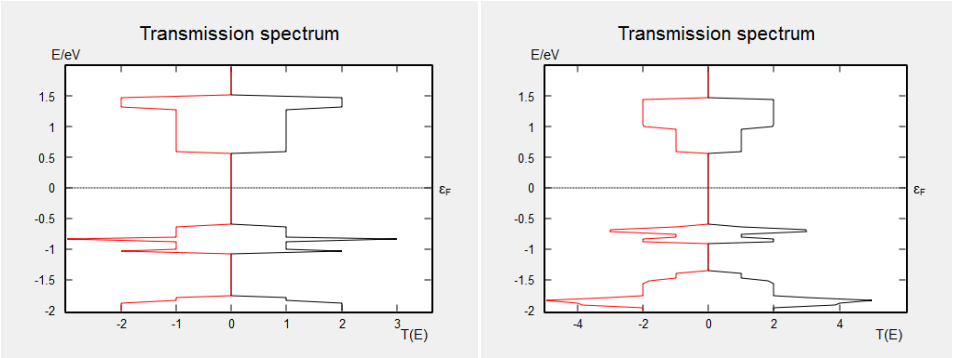


(c) (e)

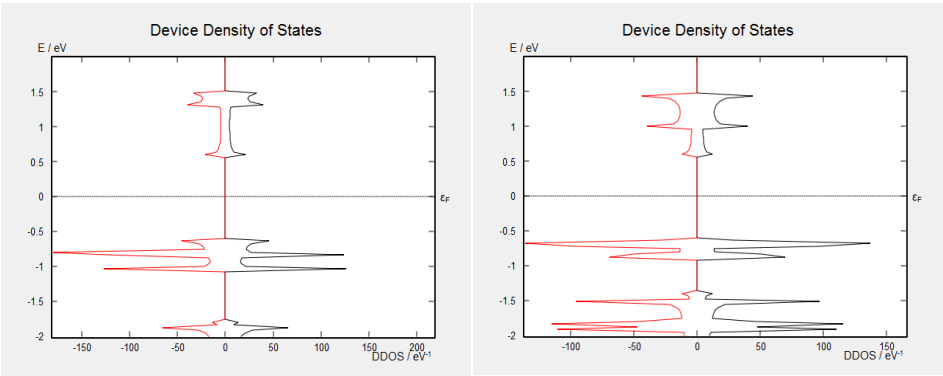


(d) (f)

Figure 4.9 The results for armchair ZnO device structure via $W_4$ and $W_6$. The geometries in (a) and (b) respectively; (c), (d) the transmission spectrum and the density of states for $W_4$; (e), (f) the transmission spectrum and the density of states for $W_6$.

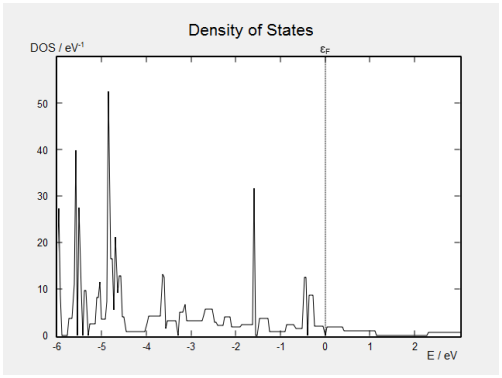


(a)

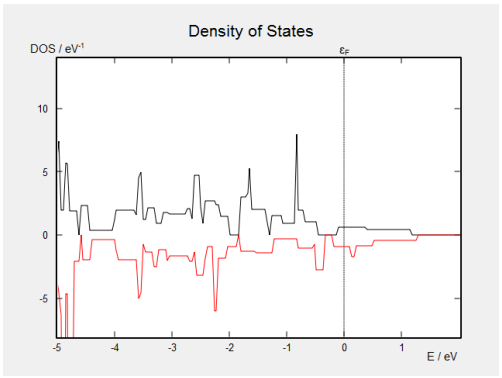


(d)

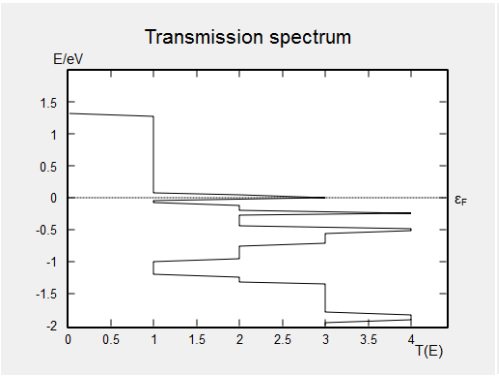


(b)

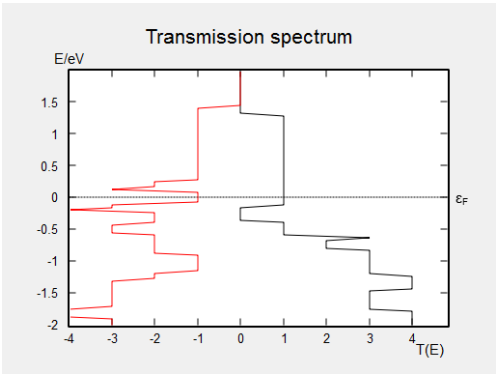


(e)

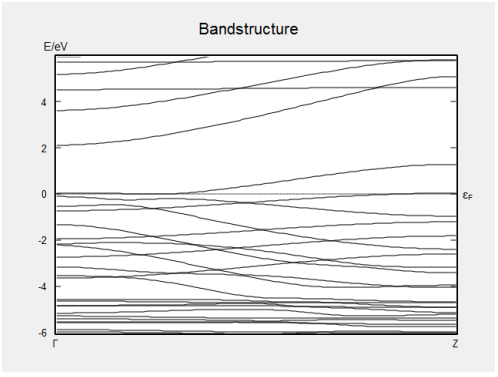


(c)

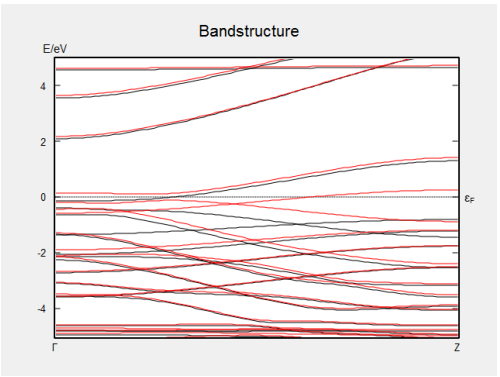


(f)

Figure 4.10 The results for the zigzag ZnO nanoribbon in the absence and presence of spin. (a), (b) and (c) are the density of states, transmission spectrum and the band structure in the absence of spin, respectively; (d), (e) and (f) density of states, transmission spectrum and the band structure in the presence of spin, respectively.

The spin independent electronic structure results of a zigzag ZnO nanoribbon are shown in Figure 4.10a,b and c. The density of states at the Fermi level is finite, which indicates the metallic behavior (Figure 4.10a). This finite value in the density of states yields a pronounced peak in the transmission probability at the Fermi energy (Figure 4.10b), implying the metallic property. The corresponding band structure exhibits the expected variation crossing the Fermi level (Figure 4.10c). The spin dependent variation for this system is illustrated in Figure 4.10d,e and f. Both the majority and minority transmission go to unity at the Fermi level (Figure 4.10e). The metallic behavior is clarified by the finite density of states for both spin orientations at the Fermi level (Figure 4.10d) and spin dependent band structure (Figure 4.10f).

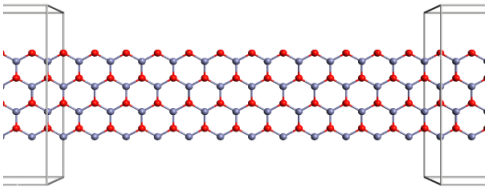

(a)

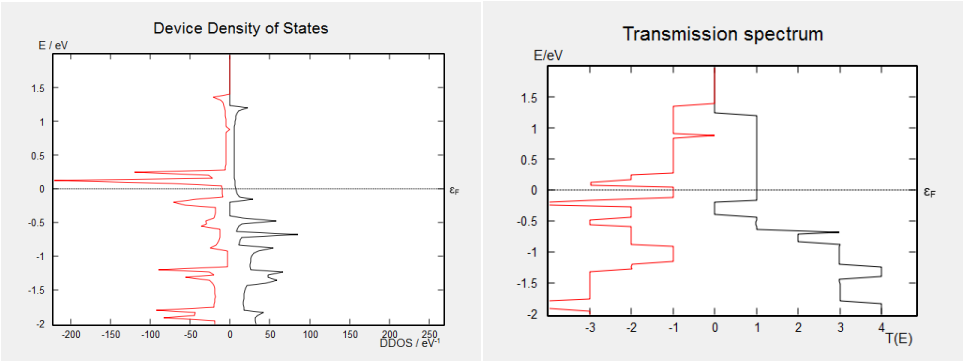


(b) (c)

Figure 4.11 The results for a zigzag ZnO nanoribbon device. (a) Zigzag ZnO device structure; (b) and (c) spin dependent density of states and transmission spectrum, respectively.

Next, we studied the properties of a zigzag ZnO device structure shown in Figure 11a. It is a metallic device which can be utilized in some cases where spin dependence is involved. Spin dependent device density of states and transmission spectra are

illustrated in Figure 4.11b and c. We observed an intriguing peak in minority density of states around 0.2 eV. The unity transmissions for both spins indicate the high transmission probability or electronic transport from left electrode to right electrode. The zero bias spin dependent conductance was obtained as $3.87\text{x}10^{-5}$ S for both majority and minority spins, giving rise to a total conductance of $7.75\text{x}10^{-5}$ S. The average magnetic moment per central atom was found to be $0.086\mu_B$. This value points out the increase in the spin dependency in the device formed by zigzag ZnO.

Finally, in order to determine the effect of ferromagnetic electrodes, we replaced the ZnO electrodes by Ni electrodes for an armchair ZnO in the central region, forming the Ni-ZnO armchair nanoribbon device (see Figure 4.12a). Using the Ni electrodes, one can inject the spin polarized electrons into the central region to induce spin polarized transport through the device. Hence we are able to observe the spin dependent variation in the spectra. In this case, the spin dependent electronic properties were found both in the presence and absence of U_correction as shown in Figure 4.12. We see the substantial change in the spin dependent density of states upon taking into account the U term (Figure 4.12b and d). It is expected because of the fact that Ni is a transition metal and has a d orbital. U term becomes especially important for atoms which have d orbitals. In order to be applicable, a spintronic device must have sufficient spin polarization, resulting in half-metallicity. A half-metallic material exposes, at the Fermi energy, a metallic property for one spin orientation and semiconducting property for the other orientation. Hence, one might need half-metallic material to propose a spintronic device. As shown in Figure 12b and d, half metallic property was almost observed for Ni-ZnO armchair nanoribbon device. In these figures, minority density of states has a finite value but majority one is almost zero, giving rise to half-metallic property or a spin polarization at the Fermi energy. The transmission for both spin orientations becomes zero at the Fermi level (see Figure 4.12c and e). The zero bias spin dependent conductance was calculated to be 1.61 nS for majority spins and 24.3 nS for minority spins, yielding a total conductance of 25.9 nS. The magnetic moment per central atom was also obtained for Ni-ZnO armchair nanoribbon device in the presence of U correction; it was 0.01 $\mu_B$, while the average magnetic moment per electrode atom and per atom were 1.21 $\mu_B$and 0.44 $\mu_B$, respectively. As expected due to the Ni electrodes, the induced magnetic moment in the device was crucially raised.

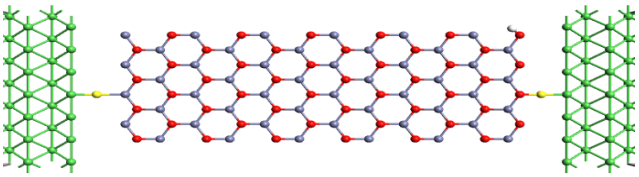

(a)

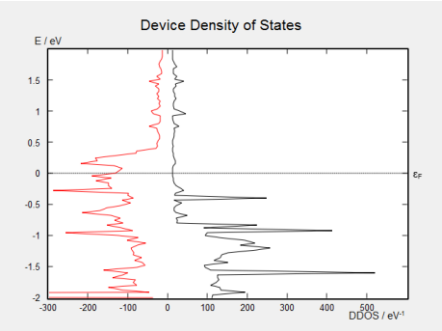


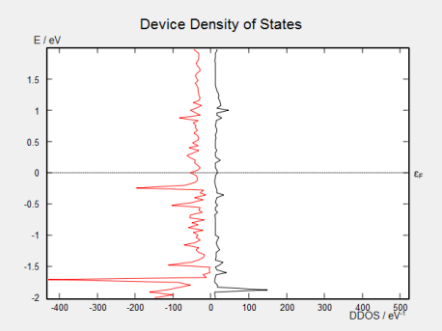


(b) (d)

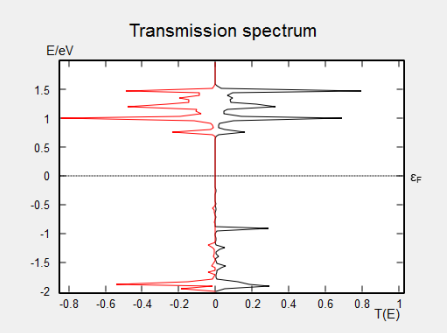


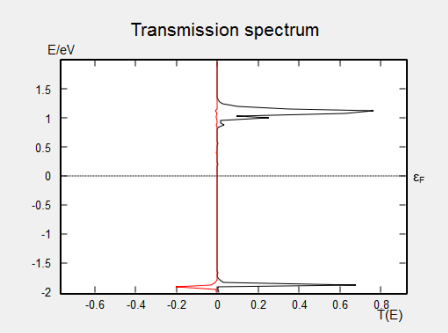


(c) (e)

Figure 4.12 The results for Ni-ZnO armchair nanoribbon device. (a) The geometry of the device; (b), (c) The density of states and the transmission spectrum in the absence of U correction; and in the presence of it (d), (e).

## 4.3 SPIN DEPENDENT ELECTRONIC and MAGNETIC PROPERTIES OF CARBON NANORIBBONS

(a) (b)

Figure 4.13 Two different geometries of a C nanoribbon. (a) The armchair C nanoribbon; (b) The zigzag C nanoribbon. The white atoms at the edges are hydrogen representing the passivation of the system.

For the sake of comparison, the same calculations above were performed on the electronic properties of armchair and zigzag C nanoribbons. Both the ZnO and C based nanoribbons have hexagonal structure and thus we can make a comparison concerning the transport and magnetic properties. In Fig 4.13 the armchair and zigzag structures of a C nanoribbon are shown, where at the edges of both armchair and zigzag structures hydrogen atoms are located for the passivation of the systems. The spin independent electronic properties of these nanoribbons are illustrated in Figure 4.14. For the armchair C nanoribbon, the absence of density of states and associated zero transmission in the vicinity of the Fermi level were clearly observed (Figure 4.14a and d). It indicates that armchair C nanoribbon has a semiconducting behavior. On the other hand, the zigzag C nanoribbon exhibits a metallic property as shown in Figure 4.14d. The pronounced peak in the transmission at the Fermi energy implies this behavior (Figure 4.14e). The direct band gap of the armchair nanoribbon was found to be 0.2 eV and expected band overlap was observed at the Fermi level for the zigzag nanoribbon (see Figure 4.14c and f).

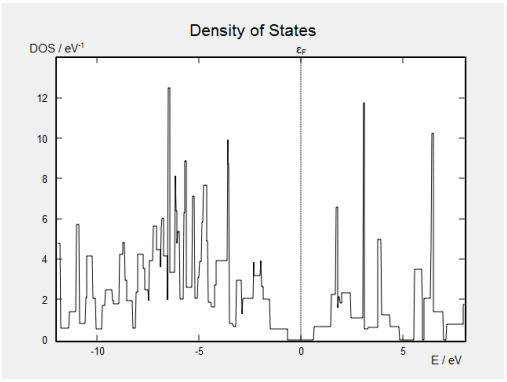


(a)

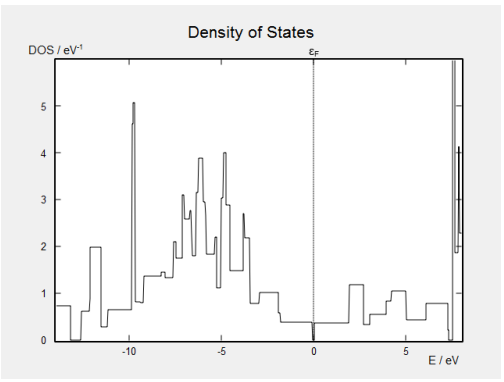


(d)

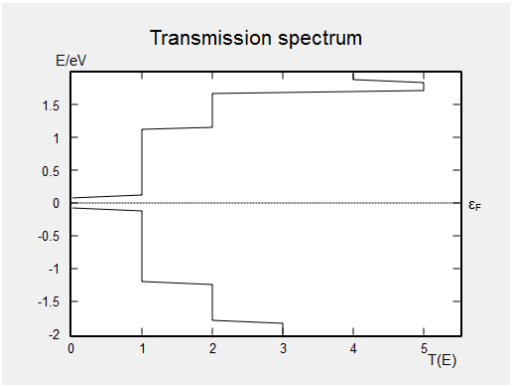


(b)

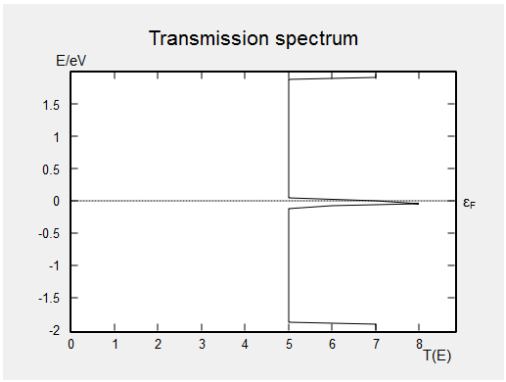


(e)

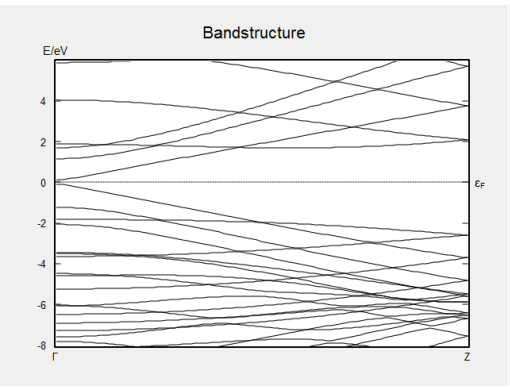


(c)

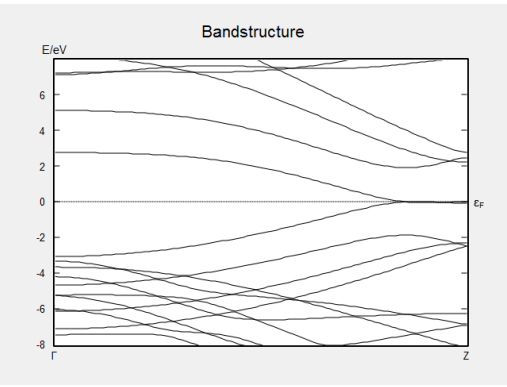


(f)

Figure 4.14 The results for C nanoribbons in the absence of spin. (a), (b), (c) The density of states, the transmission spectrum and the band structure for the armchair C nanoribbon, respectively; (d), (e), (f) The density of states, the transmission spectrum and the band structure for the zigzag C nanoribbon, respectively.

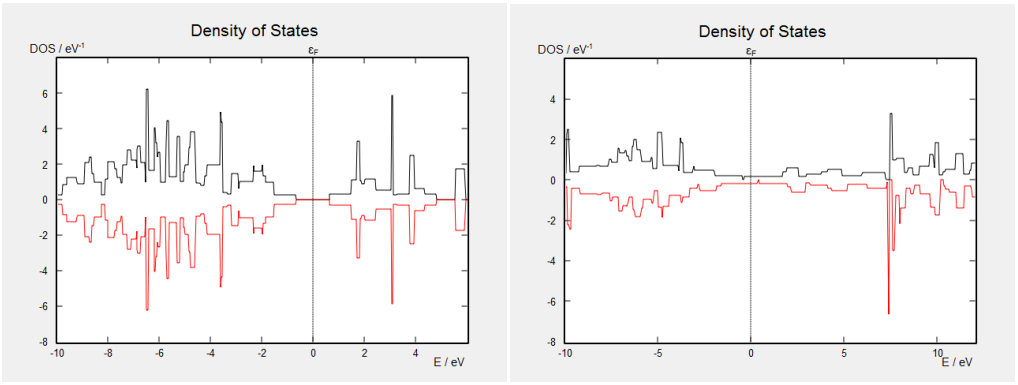


(a) (d)

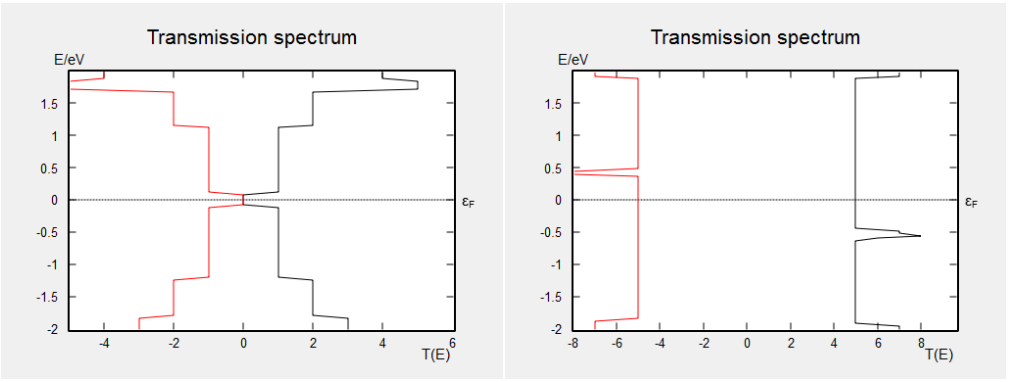


(b) (e)

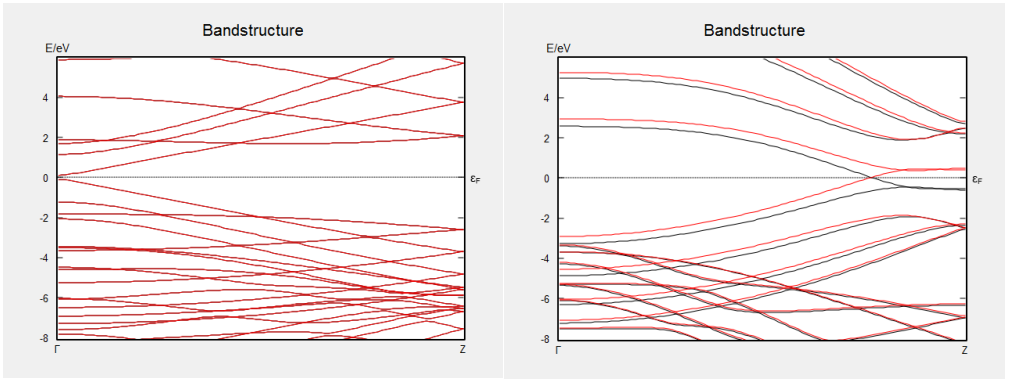


(c) (f)

Figure 4.15 The results for C nanoribbons in the presence of spin. (a), (b), (c) The density of states, the transmission spectrum and the band structure for the armchair C nanoribbon, respectively; (d), (e), (f) The density fo states, the transmission spectrum and the band structure for the zigzag C nanoribbon, respectively.

Next, we introduced the spin and obtained the spin dependent spectra and band structure as shown in Figure 4.15. It was revealed that for the armchair C nanoribbon there is a spin symmetry (Figure 4.15a,b and c), whereas for the zigzag one the spectra yields the spin resolved variation (Figure 4.15d,e and f). Thus one can infer that the geometry of a system may result in a spin dependent behavior. The shift of majority and minority peaks relative to certain energy are clearly seen in both density of states and transmission spectra (Figure 4.15d and e). For instance, a well defined minority (majority) transmission peak occurs at approximately 0.5 eV (-0.5 eV) relative to the Fermi energy.

(a) (b)

Figure 4.16 The geometries of the C nanoribbons for (a) $W_4$ and (b) $W_6$ (see the text).

As in the case of ZnO based structures, the effect of the width of C nanoribbons on the electronic properties was examined via armchair structure for $W_4$ (the width of which is 5.58 Å) and $W_6$ (the width of which is 8.04 Å) (see Figure 4.16a and b). As illustrated in the density of states spectra (Figure 4.17a and d), the semiconducting behavior around the Fermi energy is qualitatively the same with some modifications in the location and height of peaks. However, we clearly observed the distinct behavior in the transmission spectra for these structures (Figure 4.17b and e), The transmission probability increases with the increasing the width, as shown in Figure 4.17b and e, due to the increasing number of channels along the transport direction. Another difference is that for a wide energy interval there is no transmission for $W_4$ (from -1. eV to 1.75 eV)

but for $W_6$ this range was substantially reduced (from -0.5 eV to 0.5 eV). The direct band gap for $W_4$ was found to be 2.34 eV and 0.98 eV for $W_6$ (see Figure 4.17c and f). Hence the band gap increases with decreasing width as expected. Note that the band gap was 0.2 eV for the armchair naoribbon which has 8 atoms along the width. Therefore, we can deduce that electronic properties of armchair C nanoribbons depend on the width.

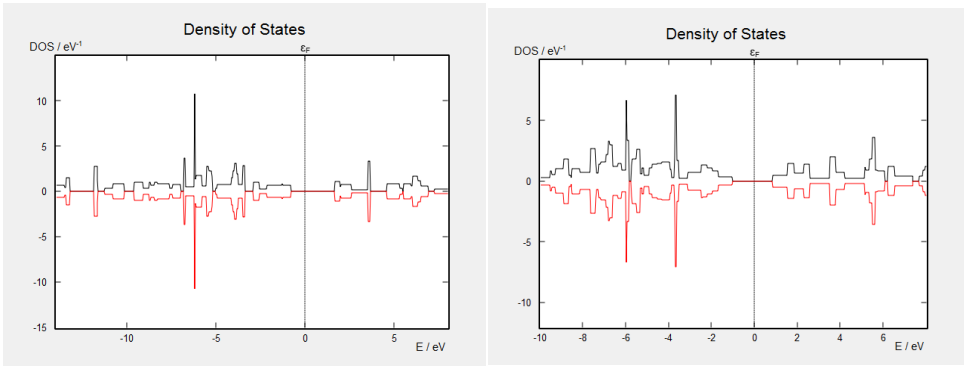


(a) (d)

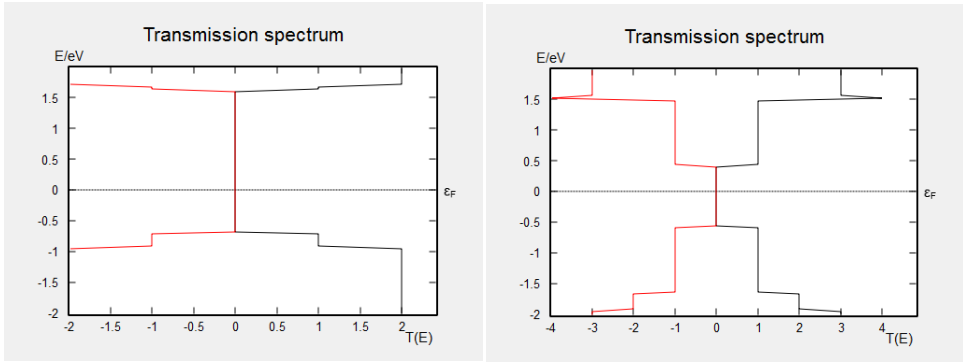


(b) (e)

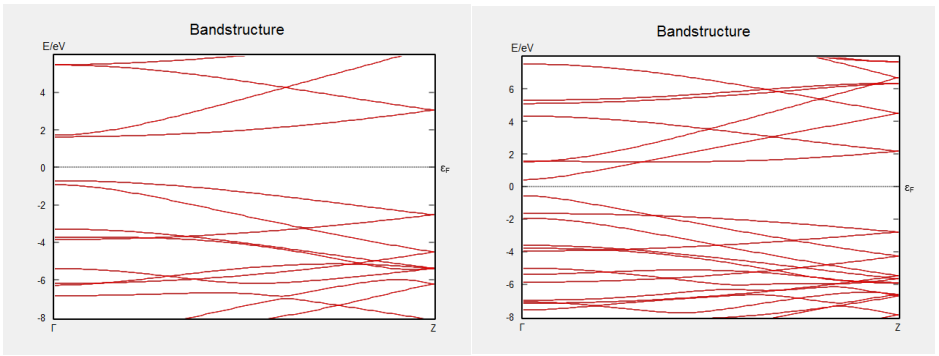


(c) (f)

Figure 4.17 The results for the armchair C nanoribbons with the widths defined by $W_4$ and $W_6$ (see the text); (a), (b), (c) Transmission spectrum, density of states and the band structure of $W_4$; (d), (e), (f) Transmssion spectrum, density of states and the band structure of $W_6$.

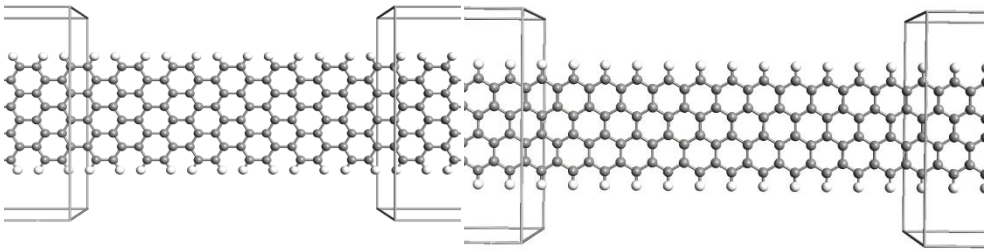

(a) (b)

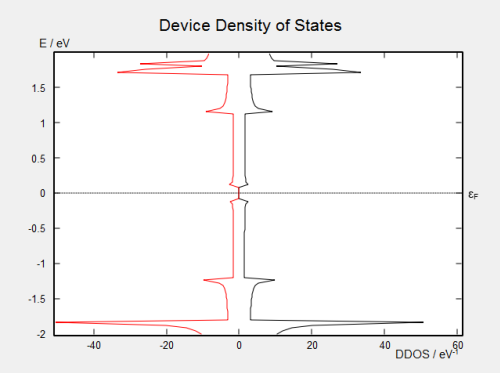


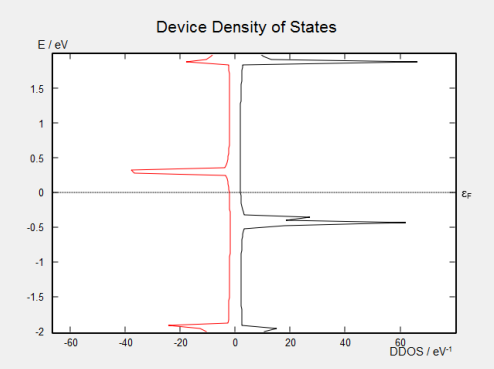


(c) (e)

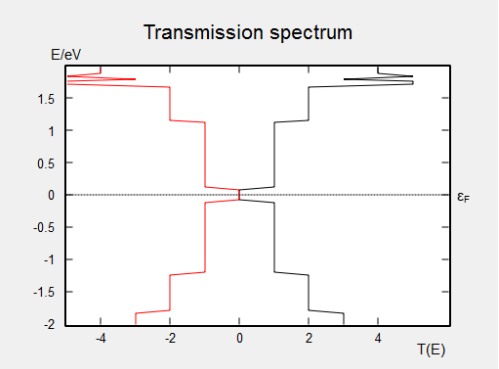


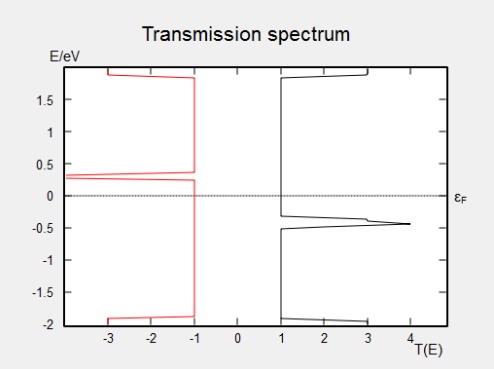


(d) (f)

Figure 4.18 The results for C nanoribbon devices. (a) Armchair C nanoribbon device; (b) Zigzag C nanoribbon device. (c), (d) The density of states and the transmission spectrum for the armchair C nanoribbon device; (e), (f) The density of states and the transmission spectrum for the zigzag C nanoribbon device.

In addition to the periodic C nanoribbons, we furthermore examined C nanoribbon devices to make a comparison with the ZnO devices (see Figure 4.18a and b). The electronic properties were obtained in the presence of spin. For the armchair C nanoribbon device, the spectra show spin symmetric variation and exhibit no states or electron transmission at the Fermi level, implying the semiconducting behavior (see Figure 4.18c and d). Moreover, its spin symmetric transmission is step like and increases with energy (Figure 4.18d). On the other hand, for the zigzag C nanoribbon device, a finite value of majority and minority density of states at the Fermi level indicates the metallic behavior as illustrated in Figure 4.18e. Besides, zigzag geometry yields a spin dependent behavior with well defined peaks at particular energies in the spectra (Figure 4.18e and f). Thus, the corresponding electronic transport becomes higher at these energies. At zero bias, both the resultant majority and minority conductance were found to be 38.7 $\mu S$, yielding a total conductance of 77.5 $\mu S$. We also calculated the average magnetic moment for the zigzag C nanoribbon device. It was implied by spin dependent shift in the spectra in Figure 4.18e and f. It was obtained as e 0.043 $\mu_B$ per central atom.

The effect of distortion on the spin dependent transport was investigated through removing a few atoms in the central region of an armchair C nanoribbon device (see Figure 4.19a). The semiconducting property is clear from the density of states spectra around the Fermi level as shown in Figure 4.19b. The spin symmetric variation remained unchanged for the distorted C nanoribbon device (Figure 4.19b and c). Due to the spin symmetry, the obtained magnetic moment was almost zero. It was $4.03 \times 10^{-5}\ \mu_B$, $-1.62\times 10^{-5}\ \mu_B$ and $2.03\times 10^{-6}\ \mu_B$ per central atom, per electrode atom and per atom, respectively.

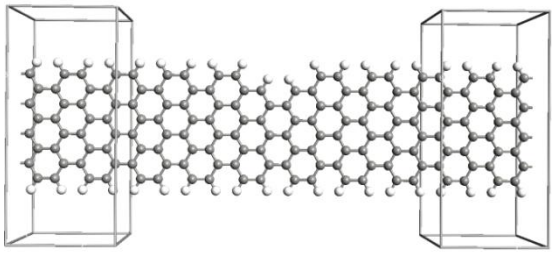

(a)

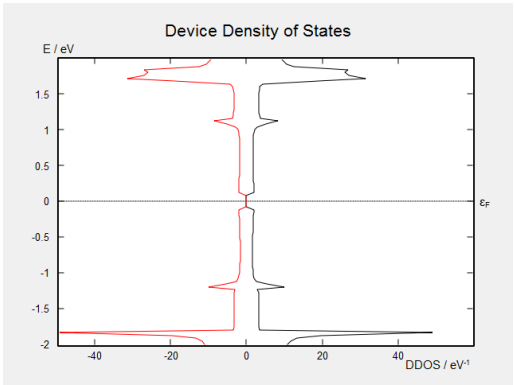


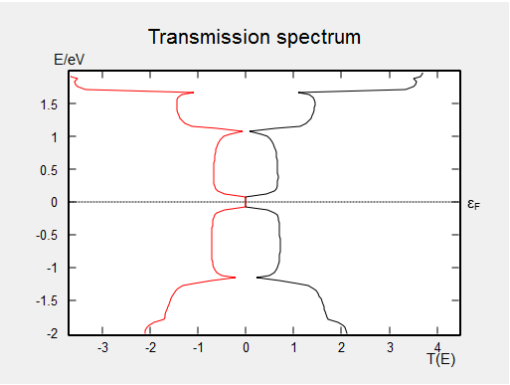


(b) (c)

Figure 4.19 The results for a distorted armchair C nanoribbon device. (a) The geometry of the device. (b) and (c) The density of states and transmission spectra of the device, respectively.

# CHAPTER 5

# CONCLUSION

We performed ab initio calculations through DFT on the armchair and zigzag ZnO nanoribbons and compared them with C nanoribbons. Introducing the Hubbard term raised the energy gap, which makes correction in the energy band gap. For the Brillouin Zone sampling, increasing the *k points* showed slight differences in the electronic structure properties. Thus, we have employed the default k-points in performing the calculations in order to get rid of time consuming.

A spin independent behavior (or spin symmetric variation) was observed in the spectra for a perfect and pure armchair ZnO nanoribbon. It has a semiconducting property with a direct band gap. Changing the width of the armchair ZnO nanoribbon exposed no crucial change in the electronic properties. Spin dependent electronic properties of an armchair ZnO device were also investigated and observed that transmission spectrum was step like and zero at the Fermi level. The average magnetic moment per central atom was almost zero due to spin symmetric behavior, yielding no spin polarization. Spin asymmetric property emerged when the distortion is introduced in the armchair ZnO nanoribbon device. Thus it was observed that it was possible to induce spin polarization through the geometry of the central region rather than via adding transition metal atoms. The effect of transition metals and Ni electrodes were examined for the armchair Ni-ZnO nanoribbon device. A half metallic property was almost observed for Ni-ZnO armchair nanoribbon device. This property is substantial in the field of spintronics, since it gives a perfect spin polarization at the Fermi energy. In this case, the induced magnetic moment in the device becomes also crucially raised. For the zigzag ZnO nanoribbons, a metallic property and, so, a finite zero bias conductance were revealed with identical spin variations (spin symmetric property). In the device structure of this system, a spin dependent shift was manifested.

This shift observed in the spectra resulted in an increase in magnetic moment, compared to the armchair ZnO device.

Both the armchair and zigzag C nanoribbons were considered for the sake of comparison. It was found that the armchair C nanoribbon had a semiconducting property, while the zigzag C nanoribbon showed metallic behavior. Hence semiconducting and metallic property are related to geometry. For an armchair geometry the system is semiconductor, but for the zigzag one it becomes metallic. When the spin was introduced, we observed a spin symmetric variation for the armchair C nanoribbon, while for the zigzag C nanoribbon a spin asymmetric behavior was obtained. As a result, the geometry has an effect on the spin dependent behavior for C nanoribbons. Besides, the electronic properties of the armchair C nanoribbons were found to be width dependent. For instance, an increase in the transmission probability and a decrease in the values of the band gap were observed while increasing the width. The corresponding device structures were also studied. When a distortion introduced in the armchair C nanoribbon device, no crucial change was found in the spin dependent electronic properties.

Our results are compatible with previous studies. For instance, single layer of zigzag ZnO nanoribbon shows metallic behavior [Topsakal, 2009] while armchair ZnO nanoribbon exhibits semiconductor property [Botello-Mendez, 2007]. In addition, the width and the thickness of the system are crucial in controlling the electronic properties of the system. Increasing the width of the system, for instance, raises the electron scattering during the electron motion [Lamba, 2012].

# REFERENCES


Atomistix ToolKit, version 2011, Quantumwise A/S (www.quantumwise.com).

Baibich, M. N., Broto, J. M., Fert, A., Nquyen Van Dau, F., Petroff, F., Etienne, P., Creuzet, G., Friederich, A., Chazelas, J., "Giant Magnetoresistance of (001) Fe/(001) Cr Magnetic Superlattices", *Physical Review Letters*, Vol. 61, pp. 2472, 1988.

Botello-Méndez, A. R., Martinez-Martinez, M. T., Lopez-Urias, F., Terrones, M., Terrones, H., "Metallic Edges in Zinc Oxide Nanoribbons", *Chemical Physics Letters*, Vol. 448, pp. 258-263, 2007.

Chambers, S. A., "A potential Role in Spintronics", *Materials Today*, Vol. 5, pp. 4, 2002.

Datta, S., Das, B., "Electronic analog of the Electrooptic Modulator", *Applied Physics Letters*, Vol. 56, pp. 665-667, 1990.

Hohenberg, P., Kohn, W., "Inhomogeneous Electron Gas", *Phys. Rev*. 136, Vol. 136, pp. B864-B871, 1964.

Hubbard, J., "Electron Correlations in Narrow Energy Bands", *Proc. R. Soc. Lond*. Vol. 276, pp. 238-257, 1963.

Jaroslav, F., " Spin's Lifetime Extended", *Nature* , Vol. 458, pp. 580-581, 2009.

Jones, R. O., Gunnarsson, O., "The Density Functional formalism, its Application and Prospects", *Rev. Mod. Phys*., Vol. 61, pp. 689-746, 1989.

Kohn, W., Sham, L. J., "Self-Consistent Equation Including Exchange and Correlation Effects", *Phys. Rev*, Vol.140, pp. A1133-A1138, 1965.

Lake, R., Klimeck, G., Bowen, R. C., Jovanovic, D., "Single and Multiband Modeling of Quantum Electron Transport Through Layered Semiconductor Devices", *American Institute of Physics*, Vol. 81, pp. 7845, 1997.

Lamba, K. V., Garg, O. P., "Modelling of Junctions between ZnO Rods/Nano Ribbons & Gold Electrods", *JECET*, Vol.1, pp. 499-504, 2012.

Landauer. R., “Spatial Variation of Currents and Fields Due to Localized Scatterers in Metallic Conduction”, *IBM*, Vol. 1, pp. 223, 1957.

Meng, H., Wang, J., “A Spintronics full adder for Magnetic CPU”, *IEEE*, Vol. 26, pp. 360-362, 2005.

Meyer, J. C., Geim, A. K., Katsnelson, M. I., Novoselov, K. S., Booth, T. J., Roth, S., “The Structures of Suspended Graphene Sheets”, *Nature* , Vol.446, pp. 60-63, 2007.

Moore, G. E.,“Gramming More Components onto Integrated Circuits”, *IEEE*, Vol. 86, pp. 82-85, 1998.

Mulliken, R. S., “Electronic Population Analysis on LCAOMO Molecular Wave Functions”, *Chem. Phys*., Vol. 23, pp. 1841, 1955.

Parr, R. G., “Density Functional Theory”, *Annual Review of Physical Chemistry*, Vol. 34, pp. 631-656, 1983.

Tiwari, J. N., Tiwari, R. N., Kim, K. S., “Zero-dimensional, One-dimensinal, Two-dimensional Nanostructuered Materials for Advanced Electrochemical Energy Devices”, *Progress in Materials Science*, Vol. 57, pp. 724-803, 2012.

Topsakal, M., Cahangirov, S., Bekaroglu, E., Ciraci, S., “First- Principle study of Zinc Oxide Honeycomb Structures”, *Physical Review B*, Vol. 80, pp. 235119, 2009.

Yuasa, S., Djayaprawira, D. D., “Giant Tunnel Magnetoresistence in Mangnetic Tunnel Junctions with a Crystalline MgO(001) Barrier” *J. Physics. D: Appl. Phys.*, Vol. 40, pp. 337, 2007.